



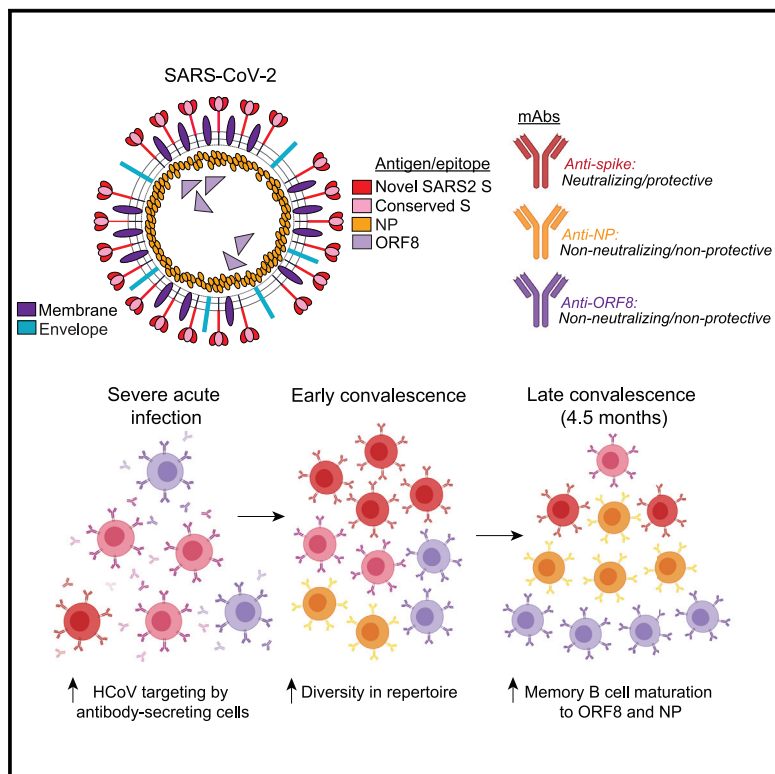
Since January 2020 Elsevier has created a COVID-19 resource centre with free information in English and Mandarin on the novel coronavirus COVID-19. The COVID-19 resource centre is hosted on Elsevier Connect, the company's public news and information website.

Elsevier hereby grants permission to make all its COVID-19-related research that is available on the COVID-19 resource centre - including this research content - immediately available in PubMed Central and other publicly funded repositories, such as the WHO COVID database with rights for unrestricted research re-use and analyses in any form or by any means with acknowledgement of the original source. These permissions are granted for free by Elsevier for as long as the COVID-19 resource centre remains active.

Immunity

Profiling B cell immunodominance after SARS-CoV-2 infection reveals antibody evolution to non-neutralizing viral targets

Graphical abstract



Authors

Haley L. Dugan,
Christopher T. Stamper, Lei Li, ...,
Daved H. Fremont, Yoshihiro Kawaoka,
Patrick C. Wilson

Correspondence

wilsonp@uchicago.edu

In brief

Dugan et al. use a multi-antigen bait sorting and single-cell sequencing approach to profile B cell immunodominance upon SARS-CoV-2 infection, revealing a dynamic response that evolves toward internal virus proteins over time. Antibodies to internal proteins were non-protective *in vivo*, highlighting the importance of vaccination for generating spike-dominated immune memory.

Highlights

- Simultaneous capture of B cell transcripts, BCR sequence, and specificity in COVID-19
- ASCs reactive to HCoV dominate the early response to severe acute infection
- MBCs targeting NP and ORF8 adapt over time and are increased in older patients
- Anti-NP and ORF8 mAbs given prophylactically in animal infection models do not protect



Article

Profiling B cell immunodominance after SARS-CoV-2 infection reveals antibody evolution to non-neutralizing viral targets

Haley L. Dugan,^{1,17} Christopher T. Stamper,^{1,17} Lei Li,^{2,17} Siriruk Changrob,² Nicholas W. Asby,³ Peter J. Halfmann,⁴ Nai-Ying Zheng,² Min Huang,² Dustin G. Shaw,¹ Mari S. Cobb,⁵ Steven A. Erickson,² Jenna J. Guthmiller,² Olivia Stovicek,² Jiaolong Wang,² Emma S. Winkler,^{6,7} Maria Lucia Madariaga,⁹ Kumaran Shanmugarajah,⁹ Maud O. Jansen,¹⁰ Fatima Amanat,¹¹ Isabelle Stewart,^{2,16} Henry A. Utset,² Jun Huang,^{1,3} Christopher A. Nelson,⁶ Ya-Nan Dai,⁶ Paige D. Hall,⁶ Robert P. Jedrzejczak,^{12,13} Andrzej Joachimiak,^{12,13,14} Florian Krammer,¹¹ Michael S. Diamond,^{6,7,8} Daved H. Fremont,⁶ Yoshihiro Kawaoka,^{4,15} and Patrick C. Wilson^{1,2,18,*}

¹Committee on Immunology, University of Chicago, Chicago, IL 60637, USA

²University of Chicago Department of Medicine, Section of Rheumatology, Chicago, IL 60637, USA

³Pritzker School of Molecular Engineering, University of Chicago, Chicago, IL 60637, USA

⁴Influenza Research Institute, Department of Pathobiological Sciences, School of Veterinary Medicine, University of Wisconsin-Madison, Madison, WI 53711

⁵Section of Genetic Medicine, University of Chicago, Chicago, IL 60637, USA

⁶Department of Medicine, Washington University School of Medicine, St Louis, MO 63130, USA

⁷Department of Pathology and Immunology, Washington University School of Medicine, St Louis, MO 63130, USA

⁸Department of Molecular Immunology, Washington University School of Medicine, St Louis, MO 63130, USA

⁹Department of Surgery, University of Chicago, Chicago, IL 60637, USA

¹⁰Department of Medicine, University of Chicago, Chicago, IL 60637, USA

¹¹Department of Microbiology, Icahn School of Medicine at Mount Sinai, New York, NY 10029, USA

¹²Center for Structural Genomics of Infectious Diseases, Consortium for Advanced Science and Engineering, University of Chicago, Chicago, IL 60637, USA

¹³Structural Biology Center, X-ray Science Division, Argonne National Laboratory, Lemont, IL 60439, USA

¹⁴Department of Biochemistry and Molecular Biology, University of Chicago, Chicago, IL 60637, USA

¹⁵Division of Virology, Department of Microbiology and Immunology, Institute of Medical Science, University of Tokyo, 108-8639 Tokyo, Japan

¹⁶Present address: School of Biological Sciences, Victoria University of Wellington, Wellington 6012, New Zealand

¹⁷These authors contributed equally

¹⁸Lead contact

*Correspondence: wilsonp@uchicago.edu

<https://doi.org/10.1016/j.immuni.2021.05.001>

SUMMARY

Dissecting the evolution of memory B cells (MBCs) against SARS-CoV-2 is critical for understanding antibody recall upon secondary exposure. Here, we used single-cell sequencing to profile SARS-CoV-2-reactive B cells in 38 COVID-19 patients. Using oligo-tagged antigen baits, we isolated B cells specific to the SARS-CoV-2 spike, nucleoprotein (NP), open reading frame 8 (ORF8), and endemic human coronavirus (HCoV) spike proteins. SARS-CoV-2 spike-specific cells were enriched in the memory compartment of acutely infected and convalescent patients several months post symptom onset. With severe acute infection, substantial populations of endemic HCoV-reactive antibody-secreting cells were identified and possessed highly mutated variable genes, signifying preexisting immunity. Finally, MBCs exhibited pronounced maturation to NP and ORF8 over time, especially in older patients. Monoclonal antibodies against these targets were non-neutralizing and non-protective *in vivo*. These findings reveal antibody adaptation to non-neutralizing intracellular antigens during infection, emphasizing the importance of vaccination for inducing neutralizing spike-specific MBCs.

INTRODUCTION

Since the emergence of SARS-CoV-2 in December 2019, the World Health Organization has reported more than 160 million infections and 3 million deaths worldwide, with these

statistics continuing to rise (World Health Organization, 2021). Faced with such persistence, the prospect of re-infection or infection with newly emerging variants warrants studies evaluating the generation of durable B cell memory upon infection.



Early in the pandemic, several independent groups identified that potently neutralizing antibodies are induced against the SARS-CoV-2 spike protein, the major antigenic glycoprotein of the virus (Chen et al., 2020; Lan et al., 2020; Robbiani et al., 2020; Wang et al., 2020; Yan et al., 2020; Yi et al., 2020). Since then, there has been a dedicated interest in the identification of durable memory B cells (MBCs) that provide protection from re-infection. Our group and others have identified MBCs against the spike, nucleoprotein (NP), and open reading frame 8 (ORF8) proteins in convalescence, and some studies show that these populations persist several months after infection (Dan et al., 2021; Guthmiller et al., 2021; Hartley et al., 2020; Rodda et al., 2021). Beyond their longevity, spike-specific MBCs continue to adapt to SARS-CoV-2 up to 6 months post-infection, in a manner consistent with antigen persistence and ongoing germinal centers (GCs) (Gaebler et al., 2021; Sakharkar et al., 2021; Sokal et al., 2021).

Despite these advances, we lack a clear understanding of MBC immunodominance and adaptation to distinct SARS-CoV-2 antigens over time and how this correlates with factors such as patient age and disease severity. Moreover, it remains to be determined whether MBCs to internal viral protein targets such as NP and ORF8 can provide protection from infection. Finally, the role of preexisting immunity to endemic human coronaviruses (HCoV) in shaping MBC responses to SARS-CoV-2 is poorly understood.

To address these knowledge gaps, we characterized the SARS-CoV-2-specific B cell repertoire in 38 COVID-19 patients, both severe acute and convalescent, approximately 1.5–4.5 months post-symptom onset, using oligo-tagged antigen bait sorting and single-cell RNA sequencing (RNA-seq). Through this approach, we provide a tool for evaluating human B cell subsets, immunodominance, and antibody adaptation to SARS-CoV-2 and have made a repository of more than 13,000 antibody sequences available to the SARS-CoV-2 research community.

Our studies reveal that MBCs display substantial reactivity toward NP and ORF8 and continue to expand and adapt to these targets over time, particularly in older patients. Although SARS-CoV-2 receptor binding domain (RBD)-specific monoclonal antibodies (mAbs) were potently neutralizing and protective, we showed that anti-NP and anti-ORF8 mAbs failed to neutralize and provide protection *in vivo*. Thus, preexisting MBC bias to non-neutralizing targets in SARS-CoV-2 could affect susceptibility to or severity of re-infection. Together, these findings highlight the importance of current SARS-CoV-2 vaccines, which are optimally formulated to induce protective MBC responses against the spike protein of SARS-CoV-2.

RESULTS

Single-cell RNA-seq reveals substantial complexity among endemic HCoV- and SARS-CoV-2-specific B cells

MBCs have potential to act as an early line of defense against viral infection, as they rapidly expand into antibody-secreting cells (ASCs) upon antigen re-encounter. To determine the landscape of MBC reactivity toward distinct SARS-CoV-2 and endemic HCoV spike viral targets, we collected peripheral blood mononuclear cells (PBMCs) and serum between April and May 2020 from 10 severely infected acute subjects and 28 subjects

upon recovery from SARS-CoV-2 viral infection (Tables S1–S4). In addition, 4 convalescent subjects returned approximately 4.5 months post-symptom onset for a second blood draw, with similar volumes of whole blood processed across time points. Severe acute infected samples were collected days 0, 1, 3, 5, and 14 before (day 0) and after receiving convalescent plasma therapy (Tables S3 and S4). All sampling time points were pooled from the same subjects for analysis because of small cell numbers.

To identify SARS-CoV-2-specific B cells, we used the SARS-CoV-2 (SARS2) spike protein, spike RBD, NP, and ORF8 to generate probes for bait-sorting enriched B cells for subsequent single-cell RNA-seq analysis. This was done by conjugating distinct PE-streptavidin (SA)-oligos (BioLegend TotalSeq) to individual biotinylated antigens (Figure 1A). To control for non-specific B cell reactivity and B cells reactive to PE, and thus improve the specificity of sorting and downstream analysis, we included an empty PE-SA-oligo, along with hantavirus PUUV, an irrelevant viral antigen control, on APC. Finally, to understand the impacts of preexisting immunity to endemic HCoV spike proteins, which share up to 30% amino acid identity with the SARS2 spike, we included a cocktail of spike proteins from four coronavirus strains that cause mild upper respiratory infections in the vast majority of individuals: HCoV-229E, HCoV-NL63, HCoV-HKU1, and HCoV-OC43, on one additional APC-SA-oligo.

From a total of 38 subjects analyzed (including four matched follow-up visits ~4.5 months post-symptom onset), we detected small percentages (0.02%–1.25%) of SARS-CoV-2-reactive total CD19⁺ B cells, which were subsequently used to prepare 5' transcriptome, immunoglobulin (Ig) VDJ, and antigen-specific probe feature libraries for sequencing (Figure 1A). We sorted on total CD19⁺ B cells with elevated mean fluorescence intensity in order to capture highly specific cells regardless of naive-like or MBC origin, though a caveat of this approach may be the exclusion of lower affinity B cells. We then integrated sequencing results from all 38 subjects using Seurat to remove batch effects and identified 16 transcriptionally distinct B cell clusters on the basis of expression profiles (Figure 1B). Adopting the ROGUE scoring method, which compares how similar all transcriptomes within a cluster are to one another, we determined that most clusters were highly pure, with the majority having a score over 0.9 (1.0 indicating 100% purity) (Figure 1C; Liu et al., 2020). We ensured that our feature libraries correlated with single-probe antigen-specific reactivity using a series of filtering steps to remove cells that were probe negative, multi-reactive and non-specific, empty PE-SA⁺, or Hanta-PUUV⁺. Because of the nature of this approach and the inability to clone antibodies from every B cell, it remains likely that a fraction of cells included in the analysis are non-specific and that a fraction of cells excluded either by gating or pre-filtering were actually specific. Therefore, our dataset represents only a subset of the total antigen-specific B cells induced by SARS-CoV-2. After all pre-filtering steps were complete, mapping only the cells that bound a single probe revealed that antigen-specific cells were enriched in distinct transcriptional clusters (Figures 1D and 1E), with considerable variation observed among individual subjects (Figures S1A and S1B). We did not identify obvious differences in B cell subset distribution or antigen reactivity in B cells from severe acute subjects analyzed early (days 0, 1, and 3) or late (days 7 and 14)

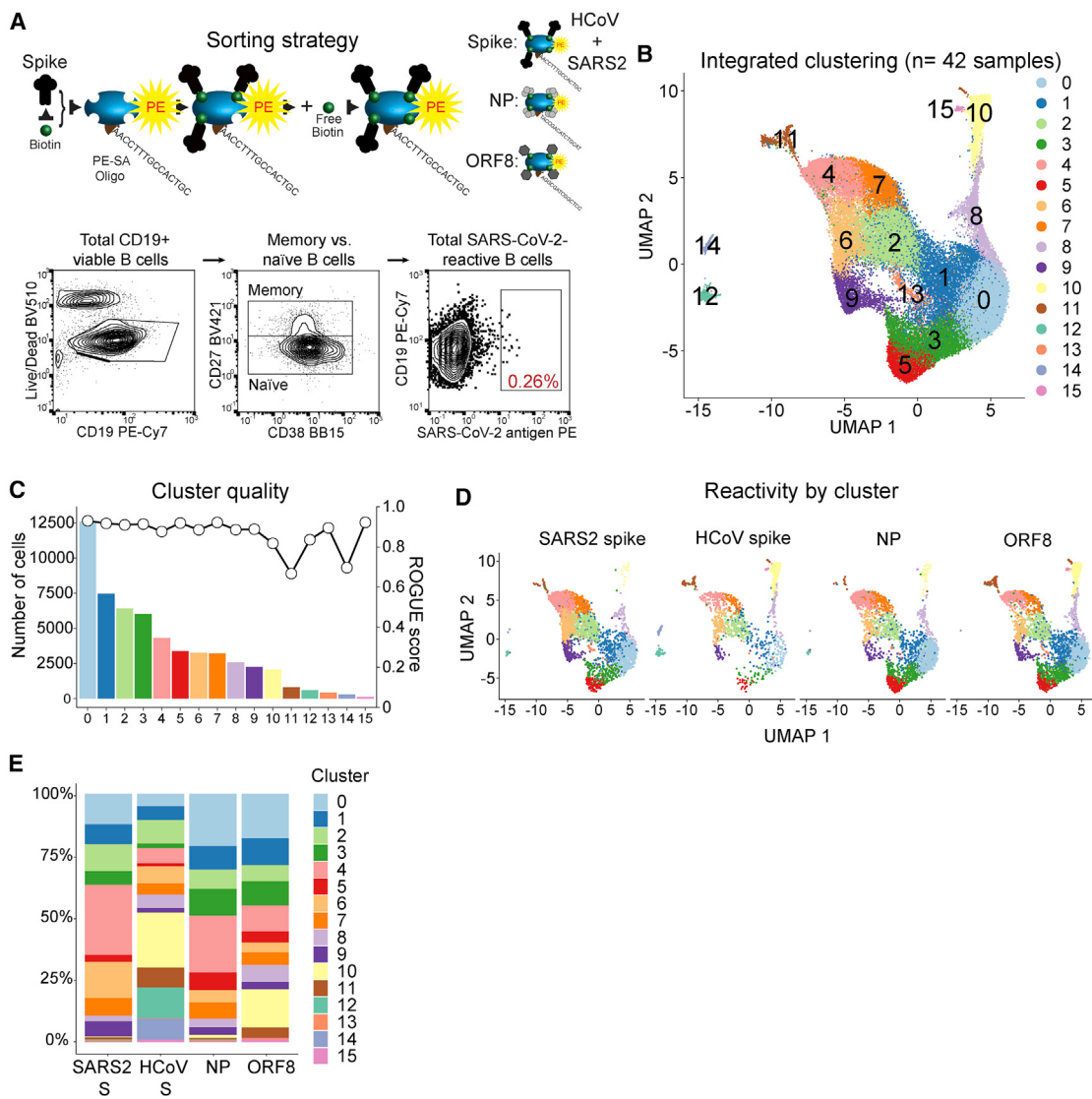


Figure 1. SARS-CoV-2-specific B cells constitute multiple distinct clusters

- (A) Model demonstrating antigen probe preparation and representative gating strategy for sorting antigen-positive B cells.
- (B) Integrated transcriptional UMAP analysis of distinct B cell clusters (n = 42 samples from severe acute [n = 10], convalescent visit 1 [n = 28], and convalescent visit 2 [n = 4] cohorts; 55,656 cells).
- (C) Cluster quality score determined by ROGUE analysis.
- (D) UMAP projections showing antigen-specific cells used in all downstream analyses and the clusters they derive from.
- (E) Quantitative visualization of antigen-specific cells and their distributions across distinct clusters.

post-convalescent plasma therapy (Figures S1C and S1D). In summary, this method revealed substantial complexity in the B cell response to distinct coronavirus antigens, which we then further dissected by subset.

The SARS-CoV-2-specific B cell landscape is defined by naive-like and MBC subsets

To discern the identity and specificity of each B cell cluster, we analyzed Ig repertoire, variable heavy (VH) chain somatic hypermutation (SHM) rates, and differentially expressed genes. Different B cell clusters varied widely in their degree of class-switch recombination (CSR) and SHM, consistent with the pres-

ence of both naive-like and memory-like B cell subsets (Figure 2A). Moreover, we quantitatively identified that targeting of viral antigens was variable across clusters (Figure 2A). To confirm B cell subset identities, we curated lists of differentially expressed genes across clusters associated with naive B cells, MBCs, recent GC emigrant cells, ASCs, and innate-like B cells (including B1 B cells and marginal zone B cells) (Figure 2B). Clusters 0, 1, 3, and 5 expressed Ig genes with little to no CSR and gene signatures associated with naive B cells, suggesting that these subsets were composed of naive-like B cells or very recently activated B cells (Figures 2A and 2B). In addition, clusters with patterns of higher CSR and SHM were further investigated for memory gene

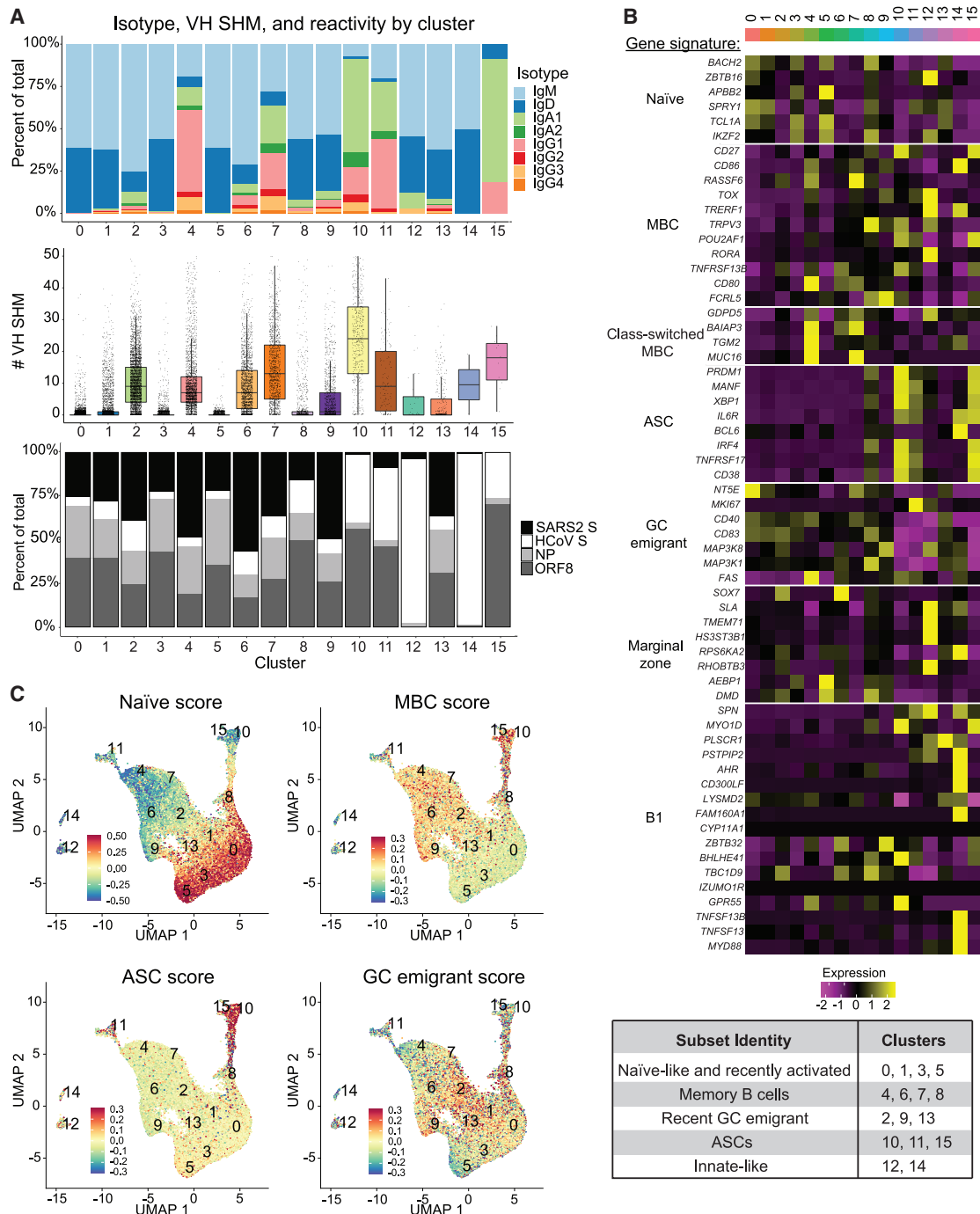


Figure 2. B cell receptor and transcriptional analysis reveals cluster identities

(A) B cell receptor isotype usage, somatic hypermutation (SHM), and antigen reactivity by cluster for all integrated samples. SHM data are plotted with the overlay indicating the median with interquartile range.

(B) Heatmap displaying differentially expressed genes across clusters. A summary of cluster identities is provided below.

(C) UMAP projections with cell color indicating gene module scoring for the indicated B cell subsets.

Also see Tables S5 and S6.

signatures. On the basis of expression of key genes (Tables S5 and S6), we identified clusters 4, 6, 7, and 8 as MBCs; clusters 2, 9, and 13 as recent memory or GC emigrants; clusters 10, 11,

and 15 as ASCs; and clusters 12 and 14 as innate-like in nature, though genes for these subsets are not well defined in humans (Figures 2A and 2B, bottom).

We generated scores for each cluster and projected them onto UMAP, allowing us to visualize how closely associated clusters relate to one another on the basis of their B cell subset score (Figure 2C). We further visualized how cells clustered on the basis of identity by overlaying key gene signatures for MBCs, recent GC emigrants, and ASCs (Table S6). Some cells were outside of their home cluster, suggesting that they were in the course of differentiation and highlighting the plasticity of cells in an active immune response (Figures S2A–S2C). ASC clusters 10, 11, and 15 displayed a high degree of SHM, suggesting that they may derive from preexisting memory that was driven against endemic HCoV spike proteins (Figure 2A). These clusters were also predominantly class-switched to IgA, an isotype most associated with mucosal immunity. To explore this possibility, we mapped the expression of genes related to mucosal surface homing and found them to be highly expressed in ASC clusters, implying that memory to past HCoV infection generates a large plasma-blast response during SARS-CoV-2 infection that re-circulates in the blood and should localize to mucosal surfaces (Figure S2D). In conclusion, we confirm that the landscape of B cell reactivity to SARS-CoV-2 and HCoV antigens is defined by distinct naive-like and MBC subsets.

B cell immunodominance and adaptability to SARS-CoV-2 and HCoVs changes with time after infection

The kinetics and evolution of B cells against the spike and non-spike antigens are poorly understood. We next investigated the dynamics of B cell subsets and their antigenic targets over time in severe acute subjects and convalescent subjects representing a range of disease severity. By color-coding cells belonging to the severe acute cohort (red), convalescent visit 1 (~1.5 months post-symptom onset; blue), and convalescent visit 2 (~4.5 months post-symptom onset; yellow) in the integrated UMAP, it became evident that distinct B cell subsets were enriched in different time points and cohorts. ASC clusters 10, 11, and 15 were derived predominantly from severe acute subjects (Figure 3A). The two convalescent time points were composed largely of naive-like and MBC clusters, with convalescent visit 2 being the most enriched for canonical class-switched MBCs (clusters 4 and 7) (Figure 3A). The severe acute cohort exhibited minimal targeting of the SARS2 spike protein and instead targeted HCoV spike and ORF8 (Figures 3B and 3C). As these ASCs were activated by SARS-CoV-2, it appeared that these were boosted MBCs with higher affinity for HCoV spikes and therefore displayed B cell receptors (BCRs) predominately loaded with HCoV spike probe when stained. In contrast, convalescent visit 1 was most enriched for SARS2 spike binding, which subsequently declined in percentage in convalescent visit 2, in which the frequency of B cells to NP and ORF8 was increased (Figures 3B and 3C).

The dynamic change observed in antigen targeting over time led us to examine antigen reactivity within distinct B cell subsets for each cohort. For the severe acute cohort, B cells binding intracellular proteins were dominated by ASC clusters, whereas SARS2 spike-specific B cells were enriched in early memory and GC emigrant B cell clusters (Figure 3D). As previously noted, HCoV spike-specific B cells were enriched in ASCs of the severe acute cohort, indicative of re-activation of preexisting immune memory. Consistent with this, HCoV spike-specific B cells

were highly mutated in the acute cohort compared with SARS2 spike-, NP-, and ORF8-specific B cells (Figure S3A).

Across the two convalescent visits, B cells reactive to ORF8 and NP were increased in percentage and absolute numbers relative to spike B cells (Figures 3E–3G; total cell numbers indicated). Although the degree of SHM for all antigen-specific B cells was increased across study visits (Figure 3H; Figures S3B and S3C), the B cells displaying the highest degree of SHM in convalescent visit 2 were majority NP-specific (Figures 3I and 3J). At the individual level, all four subjects displayed increases in the percentage of MBCs to NP across time points, and half of the subjects displayed modest increases to ORF8. The change in percentage for spike-specific B cells across visits was negligible for three of four subjects, with one subject displaying a substantial decrease (Figure S3D, S210). Previous groups have identified that spike-specific MBCs increase over time (Dan et al., 2021; Rodda et al., 2021; Sokal et al., 2021), and our study is limited in that this analysis was performed in only four subjects. However, our data support the claim that there is MBC maturation to NP and, to a lesser extent, ORF8 over time.

Analyzing isotype frequencies by antigen specificity for each cohort revealed additional differences across time points. The majority of class-switched B cells were IgA in the severe acute cohort, regardless of antigen reactivity (Figure S3E). In contrast, class switching to IgG1 was prominent for SARS2 spike-, NP-, and ORF8-reactive B cells in convalescent visit 1, while HCoV spike-reactive B cells remained largely IgA (Figure S3F). Class-switched B cells specific to the SARS2 spike declined in convalescent visit 2, and IgG1 class-switched B cells to ORF8 and NP increased in proportion (Figure S3G).

Finally, we did not identify substantial differences in serum titer to distinct antigens across convalescent visit time points (Figures S3H–S3J). Similarly, reactivity patterns in serological titer and probe hit to distinct antigens in individual subjects did not appear to be correlated (Figures S4A–S4E). This may be related to differences in B cell affinity to three-dimensional probes in the bait-sorting assay versus ELISA or the fact that the cellular response is sampled at one snapshot in time (more than 1 month post-symptom onset), with serology reflective of antibody that has accumulated since initial infection.

Together, our results point to differences in B cell immunodominance and adaptability landscapes across severe acute and convalescent cohorts, independent of serum titer. For both the severe acute cohort and convalescent visit 1 time point, SARS2 spike-specific B cells were initially the most enriched cells in memory. However, NP- and ORF8-reactive MBCs increased in proportion and showed signs of adaptation over time.

SARS-CoV-2-specific B cells display unique repertoire features and protective ability

The identification of B cells against distinct antigens is typically associated with stereotypical VH and variable light-chain kappa (VK) or variable light-chain lambda (VL) gene usages. Immunodominant and neutralizing spike and RBD epitopes are of particular interest, as they represent key targets for vaccine-induced responses. To investigate whether antigen-specific B cells displayed enriched variable gene usages, we analyzed VH and VK/VL pairs for B cells targeting HCoV spike, non-RBD spike epitopes, and RBD-specific epitopes. A B cell was considered non-RBD

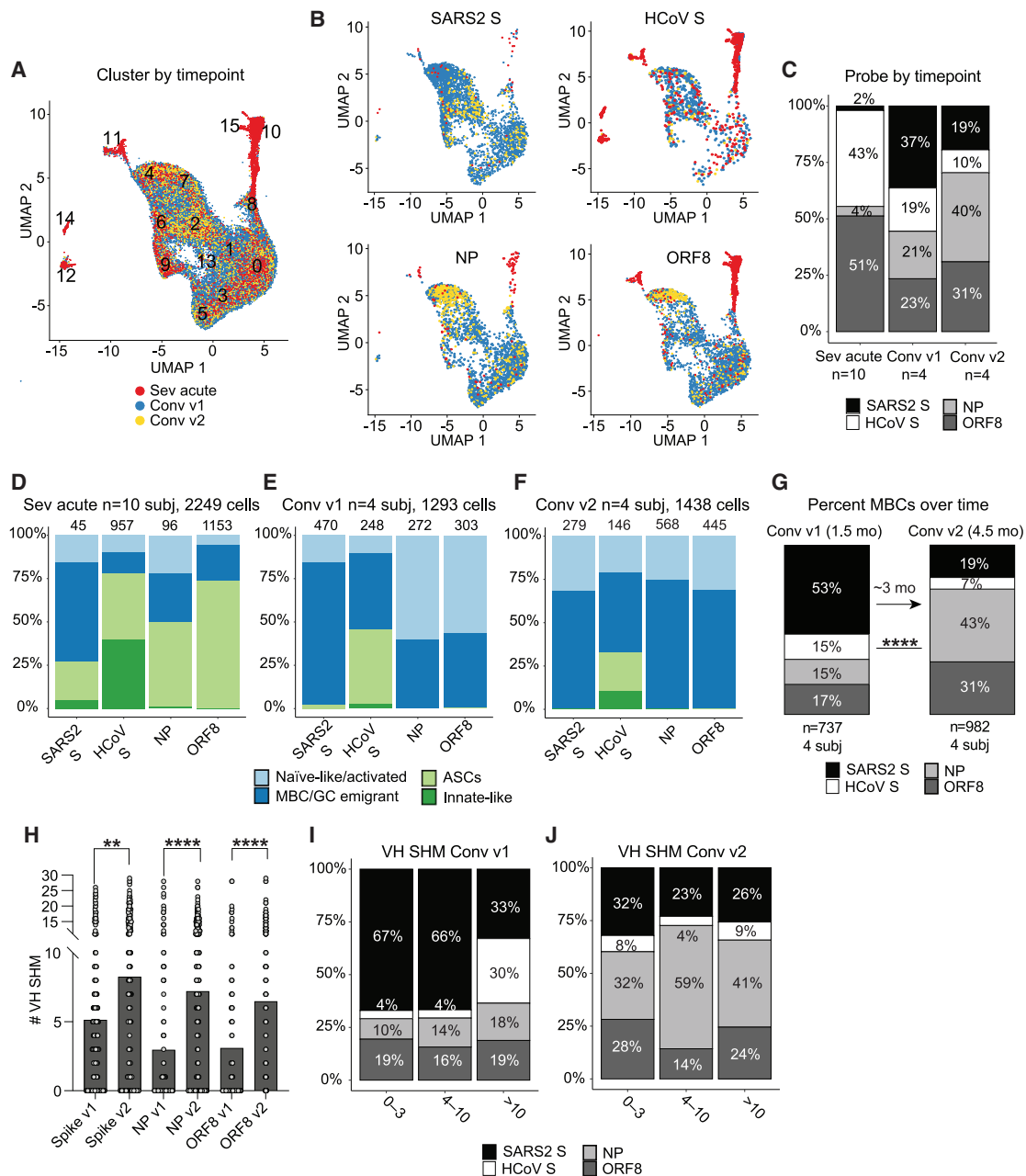


Figure 3. B cell immunodominance and adaptability landscapes vary in acute infection in convalescence

- (A) UMAP projection showing cells colored by time point of blood draw. Sev acute, severe acute; Conv v1, convalescent visit 1; Conv v2, convalescent visit 2.
- (B) UMAP projections showing cells binding the specified antigens, colored by time point of blood draw.
- (C) Percentage of B cells targeting distinct antigens by cohort. Four Conv v1 and Conv v2 subjects represent matched visits.
- (D–F) Quantification of B cell subsets targeting distinct antigens across cohorts. Also see Figure 2B, bottom for clusters used to define B cell subsets. Numbers above bars indicate the number of specific cells isolated.
- (G) Percentage of total antigen-specific memory B cells from ~1.5–4.5 months (mo) post-symptom onset in four matched-convalescent subjects. Statistics are chi-square test, ***p < 0.0001.
- (H) Variable heavy-chain (VH) somatic hypermutation (SHM) of antigen-specific B cells across both convalescent time points for four matched subjects. Statistics are unpaired non-parametric Mann-Whitney tests, **p = 0.0021 and ****p < 0.0001.
- (I and J) Antigen-specific memory B cells divided by SHM tertiles at Conv v1 (I) and Conv v2 time points (J) for four matched subjects.

spike-specific if it bound full-length spike probe and not RBD probe, and a cell that bound both RBD and full-length spike was considered to be RBD-specific. Using this approach, we found

that B cells against HCoV spike, non-SARS2 RBD spike epitopes, and the SARS2 RBD were enriched for VH1-69 gene usage (Figures 4A–4C). VH1-69 is commonly used by broadly neutralizing

antibodies against the hemagglutinin stalk domain of influenza viruses, as well as the gp120 co-receptor binding site of HIV-1, because of its ability to bind conserved hydrophobic regions of viral envelope glycoproteins (Chen et al., 2019). VH1-69 usage by B cells that cross-react to SARS-CoV-2 and HCoV has also been indicated (Wec et al., 2020). However, VH1-69 usage for B cells targeting HCoV spike and SARS2 spike non-RBD epitopes was predominantly enriched in convalescent visit 1 subjects and not convalescent visit 2, suggesting that the repertoire may continue to evolve months after infection (Figures 4A and 4B, right). However, several VH gene usages were enriched in both convalescent visits, regardless of antigen specificity. For SARS2 spike non-RBD-specific B cells, VH3-7 and VH1-24 were also commonly used, which we confirmed by characterizing cloned mAbs from our cohort (Figure 4B; Table S7). Although NP-specific B cells used similar variable gene usages as RBD-specific B cells (Figure 4D), ORF8-specific B cells were enriched for VH1-2 and VH1-3 paired with VK3-20, and enrichment for these VH genes persisted across both convalescent time points (Figure 4E). Finally, by analyzing the frequency of the top ten heavy and light chain gene pairings (total antigen-specific cells) shared across subjects for both convalescent time points, we observed variability among individual subjects and time points (Figure 4F).

To better understand antigen-specific BCRs and how antigenic reactivity relates to immune effectiveness, we next investigated the binding, neutralization potency, and *in vivo* protective ability of mAbs cloned from select BCRs. To do so, we expressed nearly 100 mAbs against the SARS2 spike, NP, and ORF8 from convalescent subjects, representing a multitude of clusters (Table S7). Cells from which to clone antibodies were chosen at random and were not chosen on the basis of specific sequence features. However, we note that the results described herein may be affected by sampling bias, as only a small subset of antigen-specific mAbs were cloned. We confirmed that cells designated as specific bound with moderate to high affinity to their corresponding antigens (Figure 5A), and cells identified as multi-reactive exhibited features of poly-reactivity or bound to PE (Figure S4F). We next tested the antibodies for viral neutralization using SARS-CoV-2/UW-001/Human/2020/Wisconsin virus plaque assays, where lower plaque-forming units (PFU) per milliliter equates to increased neutralization. Whereas 82% of mAbs to the RBD were neutralizing, including 42% exhibiting complete inhibition, only 23% of mAbs to spike regions outside of the RBD were neutralizing, and these showed relatively low potency (Figure 5B). NP- and ORF8-specific mAbs were entirely non-neutralizing (Figure 5B). Using animal models of SARS-CoV-2 infection, we confirmed that anti-RBD antibodies were therapeutically protective *in vivo*, preventing weight loss and reducing lung viral titers relative to PBS control and an irrelevant Ebola anti-GP133 mAb (Figures 5C and 5D).

Although mAbs to NP and ORF8 were non-neutralizing *in vitro*, they might still provide protection *in vivo*, potentially through Fc-mediated pathways if the proteins were exposed on the virus or cell surface at appreciable levels. However, neither ORF8-reactive mAbs nor NP-reactive mAbs conferred protection from weight loss or viral infection in the lung *in vivo* (Figures 5E–5H). Altogether, our data suggest that although B cells may continue to expand and evolve to intracellular antigens upon SARS-CoV-2

infection, B cell responses against these targets may not provide substantial protection from re-infection.

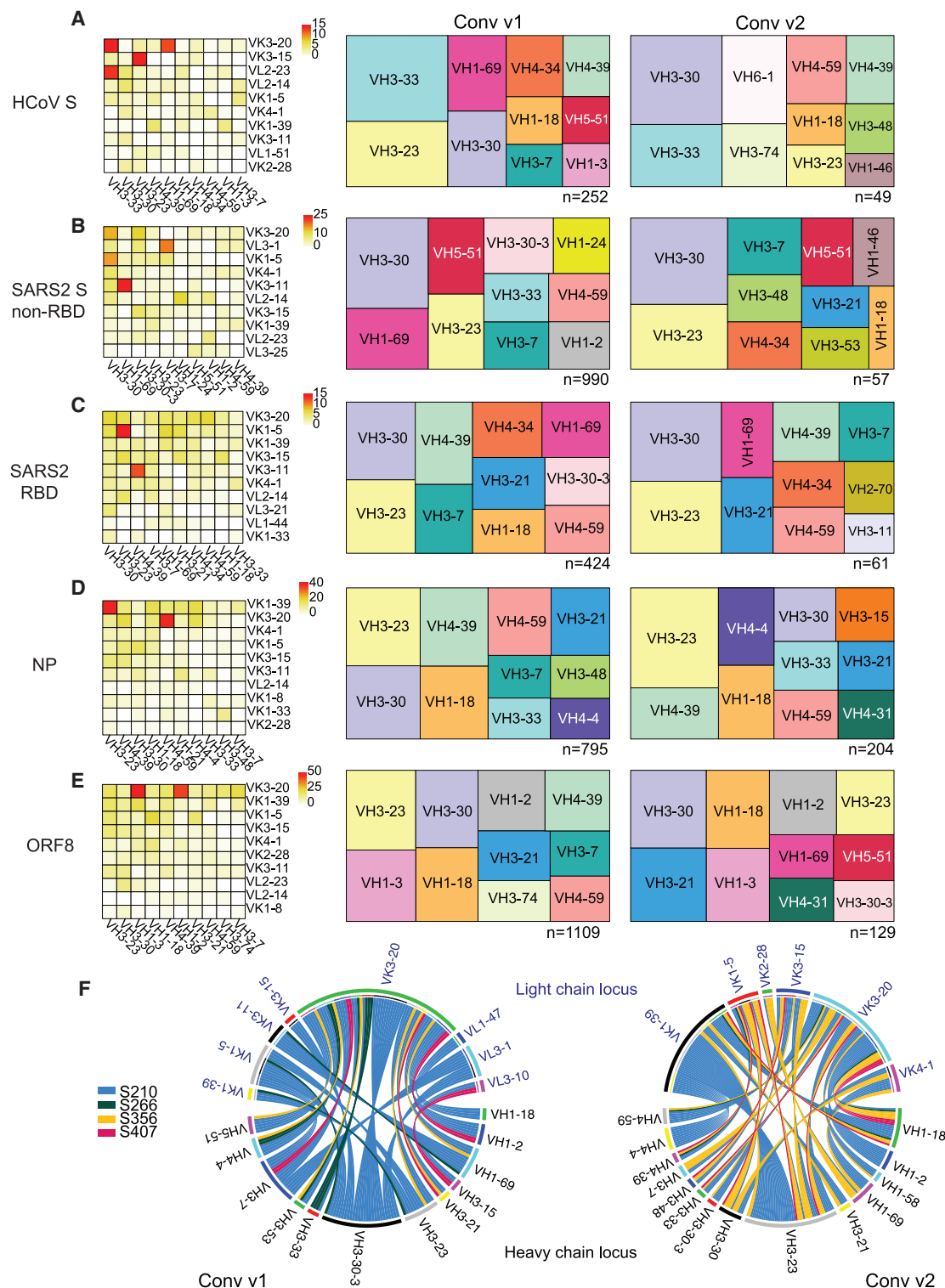
B cell immunodominance is shaped by age, sex, and disease severity

Serum antibody titers to the spike and intracellular proteins are shown to correlate with age, sex, and SARS-CoV-2 severity (Atyeo et al., 2020; Guthmiller et al., 2021; Robbiani et al., 2020). We therefore analyzed the distribution of B cell subsets and frequencies of B cells specific to the spike, NP, and ORF8 in convalescent subjects stratified by age, sex, and severity of disease. Disease severity was stratified into three categories: mild, moderate, and severe, on the basis of symptom duration and symptoms experienced (Table S1), as defined previously (Guthmiller et al., 2021).

We found that reactivity of total B cells toward different antigens varied widely by subject, likely reflecting host-intrinsic differences (Figure 6A). With age, we identified a decrease in the generation of spike-specific B cells and an increase in ORF8 and NP-specific B cells (Figure 6B). Similarly, the percentage of total spike-specific B cells was reduced in subjects with more severe disease, whereas ORF8-specific B cells were increased (Figure 6C). Last, we identified that women had increased percentages of ORF8-reactive cells, whereas men showed slightly greater percentages of NP-reactive cells (Figure 6D). To address whether differences in B cell reactivity with age and severity were associated with naive-like or MBC subsets, we analyzed reactivity by subset. We observed a substantial decrease in spike-specific MBCs and an increase in NP- and ORF8-reactive MBCs with age, while naive-like B cell subsets were more evenly distributed in reactivity across age groups (Figure 6E; Figure S5A). We identified a significant correlation with age and the percentage of ORF8-reactive MBCs in women, but not in men (Figures S5B and S5C). In contrast, the generation of specific MBCs was not different between mild and severe cases, though naive-like subsets targeting ORF8 were increased across mild, moderate, and severe disease (Figure 6F; Figure S5D).

Although B cell memory to the spike was decreased in older patients, the overall median number of VH SHMs for antigen-specific MBCs was increased relative to younger patients (Figure 6G). However, whereas the majority of MBCs harboring the most mutations targeted the SARS2 spike in younger age groups (Figures 6H and 6I), mutated MBCs against NP and ORF8 were proportionately increased relative to the spike in older patients (Figure 6J). Finally, we observed variability in the percentages of MBCs and naive-like B cells across subjects (Figure 6K), with older patients, patients with severe disease, and female patients generating reduced percentages of MBCs (Figures 6L–6N). These findings point to older patients' exhibiting poorly adapted MBC responses to the spike, instead exhibiting increased targeting and adaptation to intracellular antigens. These data are analogous to B cell responses to influenza virus vaccination in the elderly and may be attributed to the effects of immunosenescence impairing the ability to form new memory over time (Dugan et al., 2020b; Henry et al., 2019). Alternatively, these findings may reflect potential effects of preexisting immunity on the boosting of NP-specific cross-reactive MBCs.

In summary, our study highlights the diversity of B cell subsets expanded upon novel infection with SARS-CoV-2. Using this approach, we identified that B cells against the spike, ORF8,

**Figure 4. B cells targeting distinct antigens display unique variable gene usages**

(A–E) Heatmaps showing the frequency of heavy- and light-chain gene pairings for B cells binding the indicated antigens using integrated data from all cohorts (left; legend indicates number of cells per pairing), and dendograms showing the top ten variable heavy-chain (VH) gene usages for Conv v1 ($n = 28$) and Conv v2 ($n = 4$) cohorts. The number of cells encompassing the top ten VH genes represented per antigen is indicated below each dendrogram.

(F) Circos plots showing the top ten heavy- and light-chain gene pairings shared across four matched Conv v1 (left; $n = 1,293$ cells) and Conv v2 (right; $n = 1,438$ cells) subjects. Total antigen-specific cells against SARS2 spike and RBD, HCoV spike, ORF8, and NP are shown.

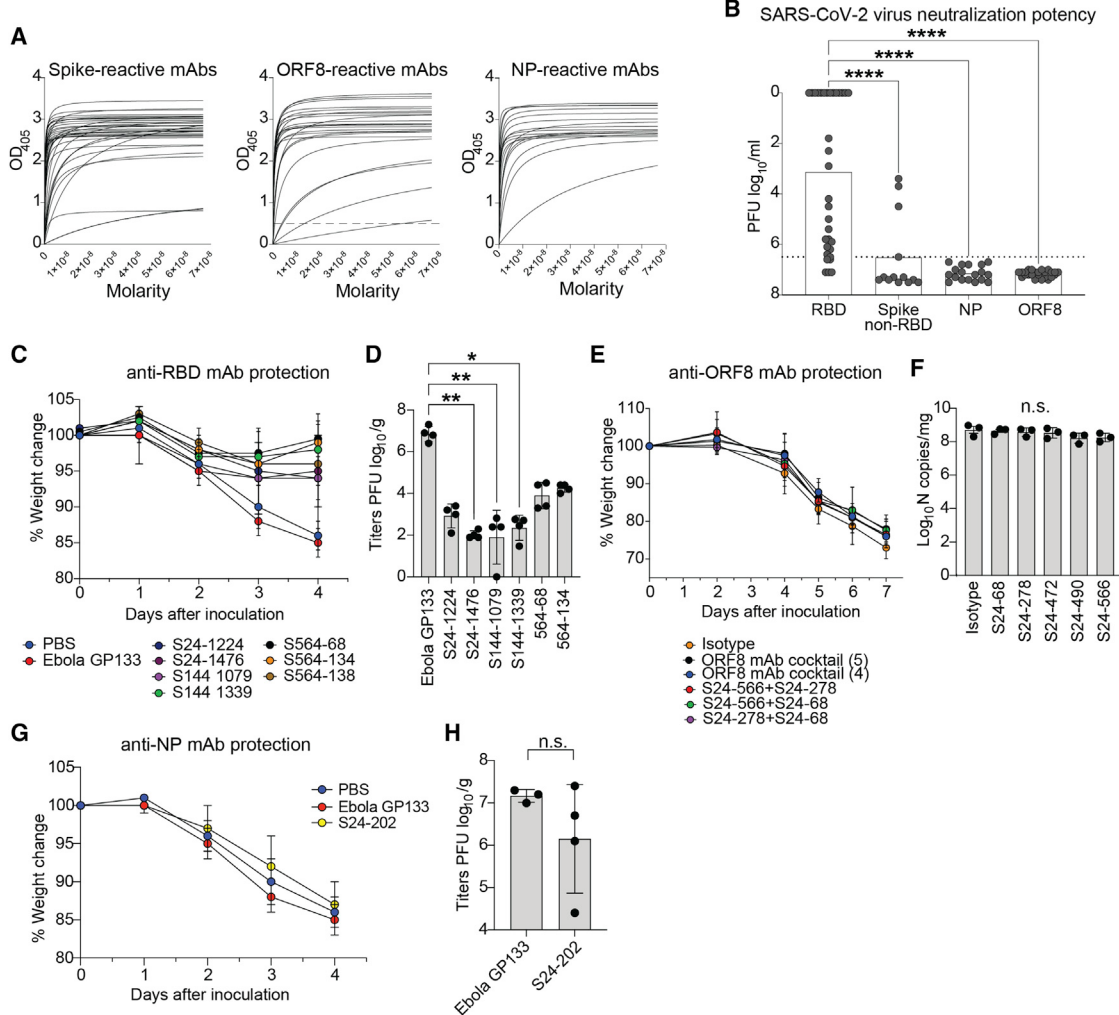


Figure 5. Neutralization capacity and *in vivo* protective ability of mAbs to the SARS-CoV-2 spike and intracellular proteins

(A) Antigen binding curves by ELISA for antigen-specific mAbs. Dashed line at $y = 0.5$ on ELISA curves represents the OD₄₀₅ cutoff of 0.5 for positivity (spike, $n = 43$; NP, $n = 19$; ORF8, $n = 24$). Data are representative of two or three independent experiments. Also see Table S7.

(B) Neutralization potency (\log_{10} PFU/ml) of mAbs tested by SARS-CoV-2 virus plaque assay. RBD, $n = 33$; spike non-RBD, $n = 13$; NP, $n = 18$; ORF8, $n = 24$. Dashed line at $x = 6.5$ indicates the cutoff for neutralization. Statistics are non-parametric Kruskal-Wallis with Dunn's post-test for multiple comparisons, *** $p < 0.0001$. Data are representative of one independent experiment.

(C) Weight change in hamsters intranasally challenged with SARS-CoV-2, followed by therapeutic intraperitoneal (i.p.) administration of anti-RBD antibodies (mean \pm SD, $n = 4$ biological replicates for each mAb). Control conditions are PBS injection or injection of an irrelevant Ebola virus anti-GP133 mAb.

(D) Viral titers of SARS-CoV-2 in lungs harvested from hamsters post-challenge in (C). Bars indicate mean \pm SD. Statistics are unpaired non-parametric Kruskal-Wallis with Dunn's post-test for multiple comparisons, * $p = 0.0135$, ** $p = 0.0011$, and ** $p = 0.0075$.

(E) Weight change of mice intranasally challenged with SARS-CoV-2, followed by therapeutic i.p. administration of anti-ORF8 antibody cocktails (mean \pm SD, $n = 3$ biological replicates for each mAb).

(F) Viral titers of SARS-CoV-2 in lungs harvested from mice post-challenge shown in (E). Titers are presented as N gene copy number compared with a standard curve, and bars indicate mean \pm SD. Statistics performed are non-parametric Kruskal-Wallis with Dunn's post-test for multiple comparisons; no differences were significant.

(G) Weight change in hamsters intranasally challenged with SARS-CoV-2, followed by therapeutic intraperitoneal (i.p.) administration of an anti-NP antibody (mean \pm SD, $n = 4$ biological replicates for each mAb).

(H) Viral titers of SARS-CoV-2 in lungs harvested from hamsters post-challenge shown in (G). Bars indicate mean \pm SD. Statistics performed are non-parametric Mann-Whitney test; no differences were significant.

and NP differ in their ability to neutralize and derive from functionally distinct and differentially adapted B cell subsets; that MBC output over time shifts from the spike to intracellular antigens; and that targeting of these antigens is affected by age, sex, and disease severity.

DISCUSSION

The COVID-19 pandemic continues to pose one of the greatest public health and policy challenges in modern history, and robust data on long-term immunity are critically needed to evaluate

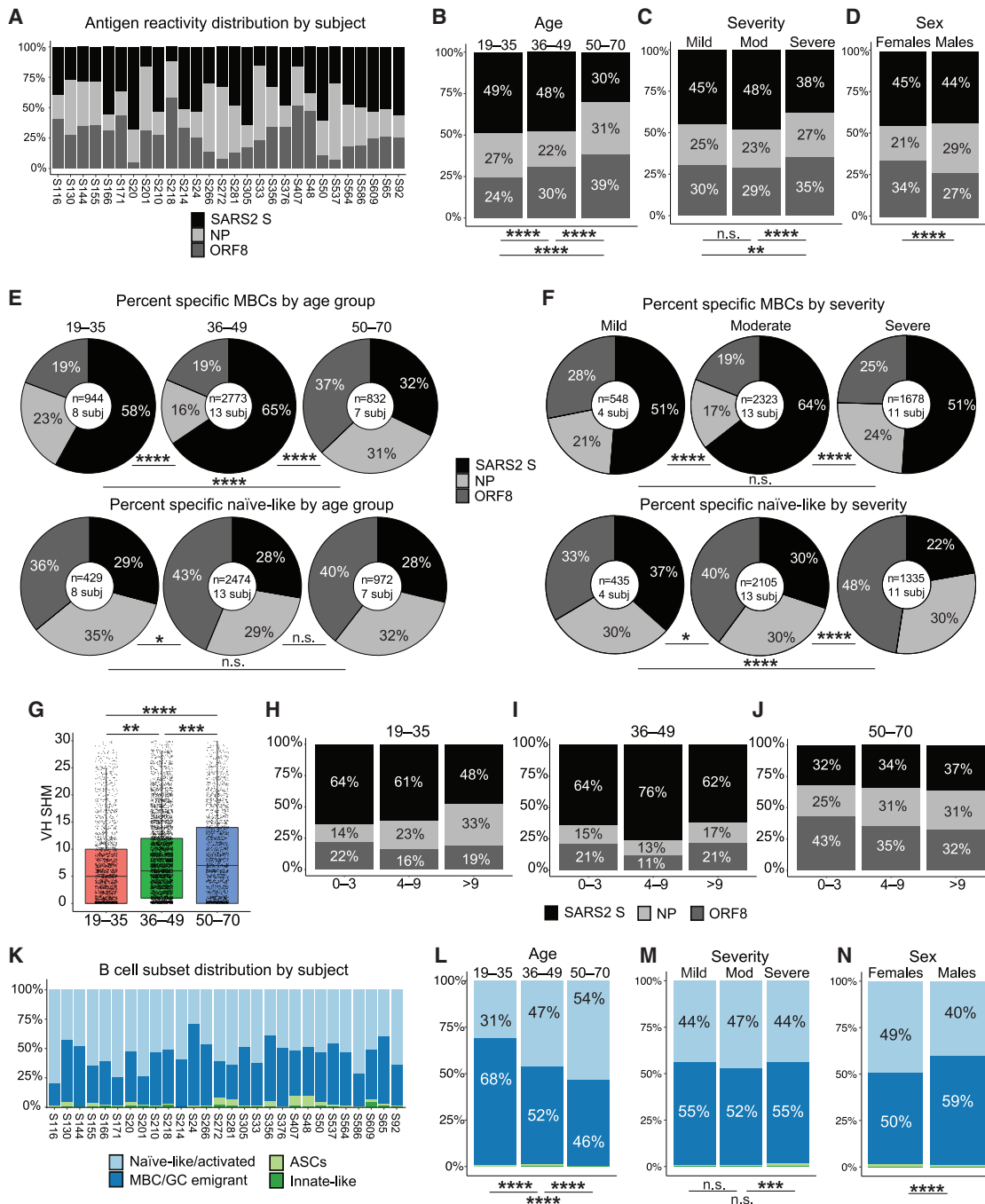


Figure 6. Antigen-specificity and B cell subset distribution is linked to clinical features

(A) Reactivity distribution of total antigen-specific B cells by subject for the convalescent visit 1 cohort ($n = 28$).

(B–D) Reactivity distribution of total antigen-specific B cells by age (B), disease severity (C), and sex (D). Statistics are chi-square post hoc tests with Holm-Bonferroni adjustment, $^{**}p = 0.0012$ and $^{***}p < 0.0001$; n.s., not significant. For age groups, 19–35 years, $n = 1,382$ cells, 8 subjects; 36–49 years, $n = 5,319$ cells, 13 subjects; 50–70 years, $n = 1,813$ cells, 7 subjects. For severity groups, mild, $n = 990$ cells, 4 subjects; moderate, $n = 4,462$ cells, 13 subjects; severe, $n = 3,062$ cells, 11 subjects. For sex, women, $n = 5,005$ cells, 14 subjects; men, $n = 3,509$ cells, 14 subjects.

(E) Reactivity of antigen-specific memory B cells (MBCs; top) or naïve B cells (bottom) by age group. Statistics are chi-square post hoc tests with Holm-Bonferroni adjustment, $^{*}p = 0.0145$ and $^{***}p < 0.0001$; n.s., not significant.

(F) Reactivity of antigen-specific MBCs (top) or naïve B cells (bottom) by disease severity. Statistics are chi-square post hoc tests with Holm-Bonferroni adjustment, $^{*}p = 0.0143$ and $^{***}p < 0.0001$; n.s., not significant.

(G) Variable heavy-chain (VH) somatic hypermutation (SHM) for MBCs by age group (overlay shows median with interquartile range). Statistics are unpaired non-parametric ANOVA with Tukey's test for multiple comparisons, $^{**}p = 0.002$, $^{***}p = 0.0008$, and $^{****}p < 0.0001$.

(legend continued on next page)

future decisions regarding COVID-19 responses. Our approach combined three powerful aspects of B cell biology to address human immunity to SARS-CoV-2: B cell transcriptome, Ig sequencing, and recombinant mAb characterization. We show that antibodies targeting key protective spike epitopes are enriched within MBC populations, but over time the MBC pool continues to adapt toward non-protective intracellular antigens, which could be a molecular hallmark of waning B-cell-mediated protection. This is further evidence that widespread vaccination, which only elicits a response to the spike, may be critical to end the pandemic.

Through this study, we revealed that the landscape of antigen targeting and B cell subsets varied widely across severe acute subjects and convalescent subjects between 1.5 and 4.5 months post-symptom onset. Severe acute patients mounted a large ASC response toward HCoV spike and ORF8, derived largely from IgA ASC populations. The expansion of highly mutated plasmablasts to HCoV spike in severe acute patients suggests that the early response to SARS-CoV-2 in some patients may be dominated by an original antigen sin response, as plasmablasts are often re-activated from preexisting memory (Dugan et al., 2020a). It remains unclear whether such responses worsen the severity of disease or reflect an inability to adapt to novel SARS2 spike epitopes. Alternatively, whether HCoV spike binding B cells adapt to the SARS2 spike and can provide protection is of interest for the potential generation of a universal coronavirus vaccine. Further investigation into the protection afforded by cross-reactive antibodies is warranted, as previous studies have identified cross-reactive HCoV and SARS1 binding antibodies can neutralize SARS-CoV-2 (Ng et al., 2020; Wec et al., 2020). Vaccine-induced responses to the spike will also be shaped by preexisting immunity and should be investigated.

Although SARS2 spike-specific B cells from the convalescent cohort were enriched in memory, we also identified MBCs and ASCs to HCoV spike, which waned 4.5 months after infection. This later time point coincided with an increase in overall numbers and percentage of ORF8- and NP-specific MBCs, which displayed a marked increase in SHM. This phenotype was pronounced in older patients, who exhibited reduced MBC targeting of the spike. Patients who were older, were female, and had more severe disease showed increased B cell targeting of ORF8, and older patients tended to generate more memory to intracellular proteins over time. We identified B cells targeting these intracellular proteins as exclusively non-neutralizing and non-protective. Mechanistically, these observations may be explained by reduced adaptability of B cells or increased reliance on CD4 T cell help for B cell activation, which have been observed in aged individuals upon viral infections and are dysregulated in aged patients (Dugan et al., 2020b; Henry et al., 2019). Furthermore, T cell responses to SARS-CoV-2 intracellular proteins are prevalent in convalescent COVID-19 patients (Grifoni et al., 2020; Le Bert et al., 2020; Peng et al., 2020). The shift in memory output during convalescence may also reflect the massive difference in pro-

tein availability, with each virion producing only dozens of spikes but thousands of intracellular proteins (Grifoni et al., 2020; Lu et al., 2021; Yao et al., 2020).

Finally, the identification of multiple distinct antigen-specific subsets of naive-like, innate-like B cells, MBCs, and ASCs illustrates the complexity of the B cell response to SARS-CoV-2, revealing an important feature of the immune response against any novel pathogen. More research is warranted to determine whether the expansion of particular antigen-specific B cell subsets directly affects susceptibility and disease severity and, conversely, whether age or disease severity shape memory formation. Addressing these questions will be critical for understanding the disease course, determining correlates of protection, and developing vaccines capable of protecting against SARS-CoV-2 and emerging variants.

Limitations of study

A primary limitation to this study is the assumption that the total number and overall distribution of antigen-specific B cells is accurately captured by the bait-sorting method described herein. These parameters could be altered by a number of factors, including probe preparation, staining dilution, flow cytometry gating, and bioinformatics analysis. However, this approach is inherently more sensitive and high throughput compared with serology and lower throughput methods for single B cell cloning. The frequencies of MBCs examined will also be dependent on the numbers that could be isolated by bait sorting starting from purified B cells, rather than examining reactivity within a controlled number of MBCs per subject. An additional limitation is that we were unable to analyze acute subjects with a range of disease severity. Finally, we were unable to obtain longitudinal samples from the same individuals across acute, early and late convalescent time points, and future longitudinal studies assessing the evolution of MBCs to SARS-CoV-2 will be important.

STAR METHODS

Detailed methods are provided in the online version of this paper and include the following:

- [KEY RESOURCES TABLE](#)
- [RESOURCE AVAILABILITY](#)
 - Lead contact
 - Materials availability
 - Data and code availability
- [EXPERIMENTAL MODEL AND SUBJECT DETAILS](#)
 - Human materials
- [METHOD DETAILS](#)
 - Recombinant proteins and probe generation
 - Antigen-specific B cell sorting
 - 10X Genomics library construction
 - Computational analyses for single cell sequencing data
 - ROGUE scoring

(H–J) Antigen-specific MBCs by age, divided by SHM tertiles.

(K) B cell subset distribution by subject.

(L–N) B cell subset distribution by age (L), disease severity (M), and sex (N). Statistics are chi-square post hoc tests with Holm-Bonferroni adjustment, ***p = 0.0007 and ****p < 0.0001; n.s., not significant. For each group, n is the same as in (B)–(D).

- Antigen probe reactivity assignment
- Gene module scoring
- Selection of antibodies for mAb synthesis
- Monoclonal antibody generation
- Enzyme-linked immunosorbent assay (ELISA)
- Polyreactivity ELISA
- Neutralization assay
- *In vivo* protection assays

● QUANTIFICATION AND STATISTICAL ANALYSIS**SUPPLEMENTAL INFORMATION**

Supplemental information can be found online at <https://doi.org/10.1016/j.immuni.2021.05.001>.

ACKNOWLEDGMENTS

This project was funded in part by the National Institute of Allergy and Infectious Diseases (NIAID); National Institutes of Health (NIH) grant numbers U19AI082724 (P.C.W.), U19AI109946 (P.C.W.), and U19AI057266 (P.C.W.); and NIAID Centers of Excellence for Influenza Research and Surveillance (CEIRS) grant HHSN272201400005C (P.C.W.). N.W.A. was supported by the Multi-disciplinary Training program in Cancer Research (MTCR) (NIH grant T32 CA009594). A.J. and R.P.J. were supported by federal funds from NIAID, NIH, and the U.S. Department of Health and Human Services under contract HHSN272201700060C. F.K. and F.A. were funded by NIAID CEIRS contract HHSN272201400008C and Collaborative Influenza Vaccine Innovation Centers (CIVIC) contract 75N93019C00051 and the generous support of the JPB Foundation, the Open Philanthropy Project (2020-21561), and other philanthropic donations. Y.K. and P.J.H. were funded by the Research Program on Emerging and Re-emerging Infectious Disease grant (JP19fk0108113) and the Japan Program for Infectious Diseases Research and Infrastructure (JP20fk0108272) of the Japan Agency for Medical Research and Development (AMED), NIAID CEIRS contract HHSN272201400008C, and CIVIC contract 75N93019C00051. D.H.F., C.A.N., Y.-N.D., and P.D.H. were supported by NIAID contracts HHSN272201700060C and 75N93019C00062. M.S.D. and E.S.W. were supported by NIH grants R01 AI157155 and F30 AI152327, respectively. We kindly thank the University of Chicago CAT Facility (RRID: SCR_017760) for their assistance and allowing us to use their facilities. We thank Dr. Nicholas Chevrier for allowing us to use the Pritzker School of Molecular Engineering's sequencing facility. We are thankful to the University of Chicago Genomics Facility (RRID: SCR_019196) for their assistance with sequencing several samples. We thank John Bivona and the staff of the Howard Taylor Ricketts Laboratory for prompt training in BSL-3 practices and procedures and for use of their facilities for severe acute infected sample collection. Last, we are appreciative of the patients who donated samples for our research purposes. The Graphical abstract was created with Biorender.com.

AUTHOR CONTRIBUTIONS

H.L.D. and C.T.S. collected samples, designed and performed experiments; generated VDJ, 5' transcriptome, and feature libraries; performed Illumina sequencing; analyzed the data; and wrote the manuscript. L.L. performed computational analyses of single-cell data and wrote the manuscript. S.C. collected samples, performed the sorting of severe acute infected subjects and Illumina sequencing, performed ELISAs, and expressed recombinant SARS-CoV-2 proteins. N.W.A. generated VDJ, 5' transcriptome, and feature libraries and performed Illumina sequencing. P.J.H. performed virus neutralization and *in vivo* protection assays with mAbs. N.-Y.Z. collected samples, expressed recombinant SARS-CoV-2 proteins, and generated mAbs. M.H. performed mAb cloning. D.G.S. and M.S.C. collected severe acute infected samples. S.A.E. performed sorting of severe acute infected subjects. J.J.G. collected samples, performed serum ELISAs, and generated the infection severity scoring system. O.S. and J.W. performed serum ELISAs. J.W. assisted in mAb generation. E.S.W. performed ORF8 mAb protection studies in mice. M.L.M., K.S., and M.O.J. coordinated the convalescent COVID-19 clin-

ical study and collected patient samples. I.S. performed ELISAs. H.A.U. collected samples and expressed recombinant SARS-CoV-2 proteins. J.H. provided funding and resources for N.W.A. to perform sequencing. F.A., C.A.N., Y.-N.D., P.D.H., D.H.F., R.P.J., A.J., and F.K. provided recombinant SARS-CoV-2 proteins. E.S.W., M.S.D., and Y.K. performed and analyzed mAb neutralization and *in vivo* protection data. P.C.W. supervised the work, analyzed the data, and wrote the manuscript.

DECLARATION OF INTERESTS

The University of Chicago has filed a patent application relating to anti-SARS-CoV-2 antibodies generated in this work, with P.C.W., H.L.D., and C.T.S. as co-inventors. Several antibodies generated from this work are being used by Now Diagnostics (Springdale, Arkansas) for the development of a diagnostic test. M.S.D. is a consultant for Inbios, Vir Biotechnology, NGM Biopharmaceuticals, and Carnival Corporation and is on the scientific advisory boards of Moderna and Immunome. The Diamond laboratory has received funding support in sponsored research agreements from Moderna, Vir Biotechnology, and Emergent BioSolutions. The Icahn School of Medicine at Mount Sinai has filed patent applications relating to SARS-CoV-2 serological assays and NDV-based SARS-CoV-2 vaccines that list F.K. as co-inventor. Mount Sinai has spun out a company, Kantaro, to market serological tests for SARS-CoV-2. F.K. has consulted for Merck and Pfizer (before 2020) and is currently consulting for Pfizer, Seqirus, and Avimex. The Krammer laboratory is also collaborating with Pfizer on animal models of SARS-CoV-2.

Received: February 17, 2021

Revised: April 6, 2021

Accepted: April 29, 2021

Published: May 6, 2021

SUPPORTING CITATIONS

The following references appear in the Supplemental Information: Axelsson et al. (2020), Basso et al. (2004), Descatoire et al. (2014), Dienz et al. (2009), Frank et al. (2009), Gallagher et al. (2007), Itoh-Nakadai et al. (2014), Kim et al. (2019), Krzyzak et al. (2016), Lightman et al. (2019), Mabbott and Gray (2014), Macias-Garcia et al. (2016), Moroney et al. (2020), Müller-Winkler et al. (2021), Ochiai et al. (2020), Palm and Henry (2019), Patzelt et al. (2018), Rothstein et al. (2013), Said et al. (2001), Schena et al. (2013), Scholzen and Gerdes (2000), Smith et al. (1995), Smulski and Eibel (2018), Uhlén et al. (2015), Villa et al. (2017), Wöhner et al. (2016), Zhao et al. (2008).

REFERENCES

- Amanat, F., Stadlbauer, D., Strohmeier, S., Nguyen, T.H.O., Chromikova, V., McMahon, M., Jiang, K., Asthagiri Arunkumar, G., Jurczyszak, D., Polanco, J., et al. (2020). A serological assay to detect SARS-CoV-2 seroconversion in humans. medRxiv.
- Andrews, S.F., Huang, Y., Kaur, K., Popova, L.I., Ho, I.Y., Pauli, N.T., Henry Dunand, C.J., Taylor, W.M., Lim, S., Huang, M., et al. (2015). Immune history profoundly affects broadly protective B cell responses to influenza. Sci. Transl. Med. 7, 316ra192.
- Atyeo, C., Fischinger, S., Zohar, T., Stein, M.D., Burke, J., Loos, C., McCulloch, D.J., Newman, K.L., Wolf, C., Yu, J., et al. (2020). Distinct early serological signatures track with SARS-CoV-2 survival. Immunity 53, 524–532.e4.
- Axelsson, S., Magnuson, A., Lange, A., Alshamari, A., Hörnquist, E.H., and Hultgren, O. (2020). A combination of the activation marker CD86 and the immune checkpoint marker B and T lymphocyte attenuator (BTLA) indicates a putative permissive activation state of B cell subtypes in healthy blood donors independent of age and sex. BMC Immunol. 21, 14.
- Basso, K., Klein, U., Niu, H., Stolovitzky, G.A., Tu, Y., Califano, A., Cattoretti, G., and Dalla-Favera, R. (2004). Tracking CD40 signaling during germinal center development. Blood 104, 4088–4096.
- Bunker, J.J., Erickson, S.A., Flynn, T.M., Henry, C., Koval, J.C., Meisel, M., Jabri, B., Antonopoulos, D.A., Wilson, P.C., and Bendelac, A. (2017). Natural

- polyreactive IgA antibodies coat the intestinal microbiota. *Science* 358, eaan6619.
- Chen, F., Tzurum, N., Wilson, I.A., and Law, M. (2019). V_H1-69 antiviral broadly neutralizing antibodies: genetics, structures, and relevance to rational vaccine design. *Curr. Opin. Virol.* 34, 149–159.
- Chen, X., Li, R., Pan, Z., Qian, C., Yang, Y., You, R., Zhao, J., Liu, P., Gao, L., Li, Z., et al. (2020). Human monoclonal antibodies block the binding of SARS-CoV-2 spike protein to angiotensin converting enzyme 2 receptor. *Cell. Mol. Immunol.* 17, 647–649.
- Dan, J.M., Mateus, J., Kato, Y., Hastie, K.M., Yu, E.D., Faliti, C.E., Grifoni, A., Ramirez, S.I., Haupt, S., Frazier, A., et al. (2021). Immunological memory to SARS-CoV-2 assessed for up to 8 months after infection. *Science* 371, eabf4063.
- Descatoire, M., Weller, S., Irtan, S., Sarnacki, S., Feuillard, J., Storck, S., Guiochon-Mantel, A., Bouligand, J., Morali, A., Cohen, J., et al. (2014). Identification of a human splenic marginal zone B cell precursor with NOTCH2-dependent differentiation properties. *J. Exp. Med.* 211, 987–1000.
- Dienz, O., Eaton, S.M., Bond, J.P., Neveu, W., Moquin, D., Noubade, R., Briso, E.M., Charland, C., Leonard, W.J., Ciliberto, G., et al. (2009). The induction of antibody production by IL-6 is indirectly mediated by IL-21 produced by CD4+ T cells. *J. Exp. Med.* 206, 69–78.
- Dugan, H.L., Guthmiller, J.J., Arevalo, P., Huang, M., Chen, Y.Q., Neu, K.E., Henry, C., Zheng, N.Y., Lan, L.Y., Tepora, M.E., et al. (2020a). Preexisting immunity shapes distinct antibody landscapes after influenza virus infection and vaccination in humans. *Sci. Transl. Med.* 12, eabd3601.
- Dugan, H.L., Henry, C., and Wilson, P.C. (2020b). Aging and influenza vaccine-induced immunity. *Cell. Immunol.* 348, 103998.
- Frank, M.J., Dawson, D.W., Bensinger, S.J., Hong, J.S., Knosp, W.M., Xu, L., Balatoni, C.E., Allen, E.L., Shen, R.R., Bar-Sagi, D., et al. (2009). Expression of sprouty2 inhibits B-cell proliferation and is epigenetically silenced in mouse and human B-cell lymphomas. *Blood* 113, 2478–2487.
- Gaebler, C., Wang, Z., Lorenzi, J.C.C., Muecksch, F., Finkin, S., Tokuyama, M., Cho, A., Jankovic, M., Schaefer-Babajew, D., Oliveira, T.Y., et al. (2021). Evolution of antibody immunity to SARS-CoV-2. *Nature* 591, 639–644.
- Gallagher, E., Enzler, T., Matsuzawa, A., Anzelon-Mills, A., Otero, D., Holzer, R., Janssen, E., Gao, M., and Karin, M. (2007). Kinase MEKK1 is required for CD40-dependent activation of the kinases Jnk and p38, germinal center formation, B cell proliferation and antibody production. *Nat. Immunol.* 8, 57–63.
- Grifoni, A., Weiskopf, D., Ramirez, S.I., Mateus, J., Dan, J.M., Moderbacher, C.R., Rawlings, S.A., Sutherland, A., Premkumar, L., Jadi, R.S., et al. (2020). Targets of T cell responses to SARS-CoV-2 coronavirus in humans with COVID-19 disease and unexposed individuals. *Cell* 181, 1489–1501.e15.
- Guthmiller, J.J., Dugan, H.L., Neu, K.E., Lan, L.Y., and Wilson, P.C. (2019). An efficient method to generate monoclonal antibodies from human B cells. *Methods Mol. Biol.* 1904, 109–145.
- Guthmiller, J.J., Lan, L.Y., Fernández-Quintero, M.L., Han, J., Utset, H.A., Bitar, D.J., Hamel, N.J., Stovicek, O., Li, L., Tepora, M., et al. (2020). Polyreactive broadly neutralizing B cells are selected to provide defense against pandemic threat influenza viruses. *Immunity* 53, 1230–1244.e5.
- Guthmiller, J.J., Stovicek, O., Wang, J., Changrob, S., Li, L., Halfmann, P., Zheng, N.Y., Utset, H., Stamper, C.T., Dugan, H.L., et al. (2021). SARS-CoV-2 infection severity is linked to superior humoral immunity against the spike. *MBio* 12, e02940-20.
- Hartley, G.E., Edwards, E.S.J., Aui, P.M., Varese, N., Stojanovic, S., McMahon, J., Peleg, A.Y., Boo, I., Drummer, H.E., Hogarth, P.M., et al. (2020). Rapid generation of durable B cell memory to SARS-CoV-2 spike and nucleocapsid proteins in COVID-19 and convalescence. *Sci. Immunol.* 5, eabf8891.
- Henry, C., Zheng, N.Y., Huang, M., Cabanov, A., Rojas, K.T., Kaur, K., Andrews, S.F., Palm, A.E., Chen, Y.Q., Li, Y., et al. (2019). Influenza virus vaccination elicits poorly adapted B cell responses in elderly individuals. *Cell Host Microbe* 25, 357–366.e6.
- Itoh-Nakadai, A., Hikota, R., Muto, A., Kometani, K., Watanabe-Matsui, M., Sato, Y., Kobayashi, M., Nakamura, A., Miura, Y., Yano, Y., et al. (2014). The transcription repressors Bach2 and Bach1 promote B cell development by repressing the myeloid program. *Nat. Immunol.* 15, 1171–1180.
- Kim, C.C., Baccarella, A.M., Bayat, A., Pepper, M., and Fontana, M.F. (2019). FCRL5⁺ memory B cells exhibit robust recall responses. *Cell Rep.* 27, 1446–1460.e4.
- Krzyzak, L., Seitz, C., Urbat, A., Hutzler, S., Ostalecki, C., Gläsner, J., Hiergeist, A., Gessner, A., Winkler, T.H., Steinkasserer, A., and Nitschke, L. (2016). CD83 modulates B cell activation and germinal center responses. *J. Immunol.* 196, 3581–3594.
- Lan, J., Ge, J., Yu, J., Shan, S., Zhou, H., Fan, S., Zhang, Q., Shi, X., Wang, Q., Zhang, L., and Wang, X. (2020). Structure of the SARS-CoV-2 spike receptor-binding domain bound to the ACE2 receptor. *Nature* 581, 215–220.
- Le Bert, N., Tan, A.T., Kunasegaran, K., Tham, C.Y.L., Hafezi, M., Chia, A., Chng, M.H.Y., Lin, M., Tan, N., Linster, M., et al. (2020). SARS-CoV-2-specific T cell immunity in cases of COVID-19 and SARS, and uninfected controls. *Nature* 584, 457–462.
- Lightman, S.M., Utley, A., and Lee, K.P. (2019). Survival of long-lived plasma cells (LLPC): piecing together the puzzle. *Front. Immunol.* 10, 965.
- Liu, B., Li, C., Li, Z., Wang, D., Ren, X., and Zhang, Z. (2020). An entropy-based metric for assessing the purity of single cell populations. *Nat. Commun.* 11, 3155.
- Lu, S., Ye, Q., Singh, D., Cao, Y., Diedrich, J.K., Yates, J.R., 3rd, Villa, E., Cleveland, D.W., and Corbett, K.D. (2021). The SARS-CoV-2 nucleocapsid phosphoprotein forms mutually exclusive condensates with RNA and the membrane-associated M protein. *Nat. Commun.* 12, 502.
- Mabbott, N.A., and Gray, D. (2014). Identification of co-expressed gene signatures in mouse B1, marginal zone and B2 B-cell populations. *Immunology* 141, 79–95.
- Macias-Garcia, A., Heizmann, B., Sellars, M., Marchal, P., Dali, H., Pasquali, J.L., Muller, S., Kastner, P., and Chan, S. (2016). Ikaros is a negative regulator of B1 cell development and function. *J. Biol. Chem.* 291, 9073–9086.
- Moroney, J.B., Vasudev, A., Pertsemidis, A., Zan, H., and Casali, P. (2020). Integrative transcriptome and chromatin landscape analysis reveals distinct epigenetic regulations in human memory B cells. *Nat. Commun.* 11, 5435.
- Müller-Winkler, J., Mitter, R., Rappe, J.C.F., Vanes, L., Schweighoffer, E., Mohammadi, H., Wack, A., and Tybulewicz, V.L.J. (2021). Critical requirement for BCR, BAFF, and BAFFR in memory B cell survival. *J. Exp. Med.* 218, e20191393.
- Nelson, C.A., Lee, C.A., and Fremont, D.H. (2014). Oxidative refolding from inclusion bodies. *Methods Mol. Biol.* 1140, 145–157.
- Nelson, C.A., Pekosz, A., Lee, C.A., Diamond, M.S., and Fremont, D.H. (2005). Structure and intracellular targeting of the SARS-coronavirus Orf7a accessory protein. *Structure* 13, 75–85.
- Ng, K.W., Faulkner, N., Cornish, G.H., Rosa, A., Harvey, R., Hussain, S., Ulferts, R., Earl, C., Wrobel, A.G., Benton, D.J., et al. (2020). Preexisting and de novo humoral immunity to SARS-CoV-2 in humans. *Science* 370, 1339–1343.
- Ochiai, K., Yamaoka, M., Swaminathan, A., Shima, H., Hiura, H., Matsumoto, M., Kurotaki, D., Nakabayashi, J., Funayama, R., Nakayama, K., et al. (2020). Chromatin protein PC4 orchestrates B cell differentiation by collaborating with IKAROS and IRF4. *Cell Rep.* 33, 108517.
- Palm, A.E., and Henry, C. (2019). Remembrance of things past: long-term B cell memory after infection and vaccination. *Front. Immunol.* 10, 1787.
- Patzelt, T., Keppler, S.J., Gorka, O., Thoene, S., Wartewig, T., Reth, M., Förster, I., Lang, R., Buchner, M., and Ruland, J. (2018). Foxp1 controls mature B cell survival and the development of follicular and B-1 B cells. *Proc. Natl. Acad. Sci. U S A* 115, 3120–3125.
- Peng, Y., Mentzer, A.J., Liu, G., Yao, X., Yin, Z., Dong, D., Dejnirattisai, W., Rostron, T., Supasa, P., Liu, C., et al. (2020). Broad and strong memory CD4(+) and CD8(+) T cells induced by SARS-CoV-2 in UK convalescent individuals following COVID-19. *Nat. Immunol.* 21, 1336–1345.
- Robbiani, D.F., Gaebler, C., Muecksch, F., Lorenzi, J.C.C., Wang, Z., Cho, A., Agudelo, M., Barnes, C.O., Gazumyan, A., Finkin, S., et al. (2020). Convergent

- antibody responses to SARS-CoV-2 in convalescent individuals. *Nature* 584, 437–442.
- Rodda, L.B., Netland, J., Shehata, L., Pruner, K.B., Morawski, P.A., Thouvenel, C.D., Takehara, K.K., Eggenberger, J., Hemann, E.A., Waterman, H.R., et al. (2021). Functional SARS-CoV-2-specific immune memory persists after mild COVID-19. *Cell* 184, 169–183.e17.
- Rothstein, T.L., Griffin, D.O., Holodick, N.E., Quach, T.D., and Kaku, H. (2013). Human B-1 cells take the stage. *Ann. N Y Acad. Sci.* 1285, 97–114.
- Said, J.W., Hoyer, K.K., French, S.W., Rosenfelt, L., Garcia-Lloret, M., Koh, P.J., Cheng, T.C., Sulur, G.G., Pinkus, G.S., Kuehl, W.M., et al. (2001). TCL1 oncogene expression in B cell subsets from lymphoid hyperplasia and distinct classes of B cell lymphoma. *Lab. Invest.* 81, 555–564.
- Sakharkar, M., Rappazzo, C.G., Wieland-Alter, W.F., Hsieh, C.L., Wrapp, D., Esterman, E.S., Kaku, C.I., Wec, A.Z., Geoghegan, J.C., McLellan, J.S., et al. (2021). Prolonged evolution of the human B cell response to SARS-CoV-2 infection. *Sci. Immunol.* 6, eabg6916.
- Schena, F., Volpi, S., Faliti, C.E., Penco, F., Santi, S., Proietti, M., Schenk, U., Damonte, G., Salis, A., Bellotti, M., et al. (2013). Dependence of immunoglobulin class switch recombination in B cells on vesicular release of ATP and CD73 ectonucleotidase activity. *Cell Rep.* 3, 1824–1831.
- Scholzen, T., and Gerdes, J. (2000). The Ki-67 protein: from the known and the unknown. *J. Cell. Physiol.* 182, 311–322.
- Shlomchik, M.J., Aucoin, A.H., Pisetsky, D.S., and Weigert, M.G. (1987). Structure and function of anti-DNA autoantibodies derived from a single autoimmune mouse. *Proc. Natl. Acad. Sci. U S A* 84, 9150–9154.
- Smith, K.G., Nossal, G.J., and Tarlinton, D.M. (1995). FAS is highly expressed in the germinal center but is not required for regulation of the B-cell response to antigen. *Proc. Natl. Acad. Sci. U S A* 92, 11628–11632.
- Smulski, C.R., and Eibel, H. (2018). BAFF and BAFF-receptor in B cell selection and survival. *Front. Immunol.* 9, 2285.
- Sokal, A., Chappert, P., Barba-Spaeth, G., Roeser, A., Fourati, S., Azaoui, I., Vandenberghe, A., Fernandez, I., Meola, A., Bouvier-Alias, M., et al. (2021). Maturation and persistence of the anti-SARS-CoV-2 memory B cell response. *Cell* 184, 1201–1213.e14.
- Stadlbauer, D., Amanat, F., Chromikova, V., Jiang, K., Strohmeier, S., Arunkumar, G.A., Tan, J., Bhavsar, D., Capuano, C., Kirkpatrick, E., et al. (2020). SARS-CoV-2 seroconversion in humans: a detailed protocol for a serological assay, antigen production, and test setup. *Curr. Protoc. Microbiol.* 57, e100.
- Stuart, T., Butler, A., Hoffman, P., Hafemeister, C., Papalexi, E., Mauck, W.M., 3rd, Hao, Y., Stoeckius, M., Smibert, P., and Satija, R. (2019). Comprehensive integration of single-cell data. *Cell* 177, 1888–1902.e21.
- Uhlén, M., Fagerberg, L., Hallström, B.M., Lindskog, C., Oksvold, P., Mardinoglu, A., Sivertsson, Å., Kampf, C., Sjöstedt, E., Asplund, A., et al. (2015). Proteomics. Tissue-based map of the human proteome. *Science* 347, 1260419.
- Villa, M., Gialitakis, M., Tolaini, M., Ahlfors, H., Henderson, C.J., Wolf, C.R., Brink, R., and Stockinger, B. (2017). Aryl hydrocarbon receptor is required for optimal B-cell proliferation. *EMBO J.* 36, 116–128.
- Wang, C., Li, W., Drabek, D., Okba, N.M.A., van Haperen, R., Osterhaus, A.D.M.E., van Kuppevelde, F.J.M., Haagmans, B.L., Grosveld, F., and Bosch, B.J. (2020). A human monoclonal antibody blocking SARS-CoV-2 infection. *Nat. Commun.* 11, 2251.
- Wee, A.Z., Wrapp, D., Herbert, A.S., Maurer, D.P., Haslwanter, D., Sakharkar, M., Jangra, R.K., Dieterle, M.E., Lilov, A., Huang, D., et al. (2020). Broad neutralization of SARS-related viruses by human monoclonal antibodies. *Science* 369, 731–736.
- Winkler, E.S., Bailey, A.L., Kafai, N.M., Nair, S., McCune, B.T., Yu, J., Fox, J.M., Chen, R.E., Earnest, J.T., Keeler, S.P., et al. (2020). Publisher correction: SARS-CoV-2 infection of human ACE2-transgenic mice causes severe lung inflammation and impaired function. *Nat. Immunol.* 21, 1470.
- Wöhner, M., Tagoh, H., Bilic, I., Jaritz, M., Poliakova, D.K., Fischer, M., and Busslinger, M. (2016). Molecular functions of the transcription factors E2A and E2-2 in controlling germinal center B cell and plasma cell development. *J. Exp. Med.* 213, 1201–1221.
- World Health Organization (2021). WHO Coronavirus (COVID-19) Dashboard. <https://covid19.who.int/>.
- Yan, R., Zhang, Y., Li, Y., Xia, L., Guo, Y., and Zhou, Q. (2020). Structural basis for the recognition of SARS-CoV-2 by full-length human ACE2. *Science* 367, 1444–1448.
- Yao, H., Song, Y., Chen, Y., Wu, N., Xu, J., Sun, C., Zhang, J., Weng, T., Zhang, Z., Wu, Z., et al. (2020). Molecular architecture of the SARS-CoV-2 virus. *Cell* 183, 730–738.e13.
- Yi, C., Sun, X., Ye, J., Ding, L., Liu, M., Yang, Z., Lu, X., Zhang, Y., Ma, L., Gu, W., et al. (2020). Key residues of the receptor binding motif in the spike protein of SARS-CoV-2 that interact with ACE2 and neutralizing antibodies. *Cell. Mol. Immunol.* 17, 621–630.
- Zhao, C., Inoue, J., Imoto, I., Otsuki, T., Iida, S., Ueda, R., and Inazawa, J. (2008). POU2AF1, an amplification target at 11q23, promotes growth of multiple myeloma cells by directly regulating expression of a B-cell maturation factor, TNFRSF17. *Oncogene* 27, 63–75.

STAR★METHODS

KEY RESOURCES TABLE

REAGENT or RESOURCE	SOURCE	IDENTIFIER
Antibodies		
TotalSeq-C 0951 PE Streptavidin	Biolegend	Cat# 405261 - Lot# B313967
TotalSeq-C 0952 PE Streptavidin	Biolegend	Cat# 405263 - Lot# B308305
TotalSeq-C 0953 PE Streptavidin	Biolegend	Cat# 405265 - Lot# B308299
TotalSeq-C 0954 PE Streptavidin	Biolegend	Cat# 405267 - Lot# B294413
TotalSeq-C 0955 PE Streptavidin	Biolegend	Cat# 405269 - Lot# B308862
TotalSeq-C 0956 APC Streptavidin	Biolegend	Cat# 405283 - Lot# B314687
TotalSeq-C 0957 APC Streptavidin	Biolegend	Cat# 405285 - Lot# B314686
TotalSeq-C 0958 APC Streptavidin	Biolegend	Cat# 405293 - Lot# B320055
TotalSeq-C 0959 APC Streptavidin	Biolegend	Cat# 405159 - Lot# B323806
TotalSeq-C 0971 Streptavidin	Biolegend	Cat# 405271
PE/Cy7 anti-Human CD19 (Clone: HIB19)	Biolegend	Cat# 302215 - Lot# B242978; RRID: AB_314245
Brilliant Violet 421 anti-human CD27 (Clone: O323)	Biolegend	Cat# 302823 - Lot# B255089; RRID: AB_10900425
BV510 Mouse Anti-Human CD3 (Clone UCHT1)	BD Biosciences	Cat#563109; RRID:AB_2732053
BB515 Mouse Anti-Human CD38 (Clone: HIT2)	BD Biosciences	Cat# 564499 - Lot# 9353306; RRID: AB_2744374
Goat anti-human IgG (Fab-specific) HRP	Sigma	Cat# A0293; RRID: AB_257875
Goat anti-human IgM-HRP	Sigma	Cat# A6907; RRID: AB_258318
Goat anti-human IgA-HRP	Sigma	Cat# A0295; RRID: AB_257876
Goat anti-human IgG-HRP	Jackson Immunoresearch	Cat# 109-035-098; RRID: AB_2337586
Mouse anti-human IgG1 Fc-HRP	Southern Biotech	Cat# 9054-05; RRID: AB_2796619
Mouse anti-human IgG2 Fc-HRP	Southern Biotech	Cat# 9080-05; RRID: AB_2796633
Mouse anti-human IgG3 Hinge-HRP	Southern Biotech	Cat# 9210-05; RRID: AB_2796699
Mouse anti-human IgG4 Fc-HRP	Southern Biotech	Cat# 9200-05; RRID: AB_2796691
Mouse anti-human IgA1-HRP	Southern Biotech	Cat# 9130-05; RRID: AB_2796654
Mouse anti-human IgA2-HRP	Southern Biotech	Cat# 9140-05; RRID: AB_2796662
Goat anti-human IgD-HRP	Southern Biotech	Cat# 2030-05; RRID: AB_2795627
Goat anti-human IgG-biotin	Mabtech	Cat# 3820-4-250
Goat anti-human IgA-biotin	Southern Biotech	Cat# 2050-08; RRID: AB_2795706
Streptavidin-AP	Southern Biotech	Cat# 7100-04
EasySep Human Pan-B Cell Enrichment Kit	StemCell Technologies	Cat#19554
Bacterial and virus strains		
SARS-CoV-2/UW-001/Human/2020/Wisconsin (UW-001)	This paper, Yoshihiro Kawaoka's laboratory stock	N/A
SARS-CoV-2 (strain 2019 n-CoV/USA_WA1/2020)	CDC/BEI Resources	NR52281
NEB 5-alpha Competent <i>E. coli</i>	NEB	Cat# C2988J
Biological samples		
PBMCs from SARS-CoV-2 convalescent subjects	University of Chicago Medical Center Convalescent Plasma Project	N/A
PBMCs from SARS-CoV-2 severe acutely infected subjects	University of Chicago Medical Center Convalescent Plasma Project	N/A

(Continued on next page)

Continued

REAGENT or RESOURCE	SOURCE	IDENTIFIER
Serum from SARS-CoV-2 convalescent subjects	University of Chicago Medical Center Convalescent Plasma Project	N/A
Chemicals, peptides, and recombinant proteins		
SARS-CoV-2 Spike	Amanat et al., 2020; Stadlbauer et al., 2020	N/A
SARS-CoV-2 RBD	Amanat et al., 2020; Stadlbauer et al., 2020	N/A
SARS-CoV-2 NP RNA binding domain	This paper, Andrzej Joachimiak's laboratory stock	N/A
SARS-CoV-2 ORF8b	This paper, Daved Fremont's laboratory stock	N/A
Hantavirus PuuV glycoprotein	This paper, Florian Krammer's laboratory stock	N/A
HCoV-229E Spike	SinoBiological	Cat# 40605-V08B
HCoV-NL63 Spike	SinoBiological	Cat# 40604-V08B
HCoV-HKU1 Spike	SinoBiological	Cat# 40606-V08B
HCoV-OC43 Spike	SinoBiological	Cat# 40607-V08B
SARS-CoV-2 N F: 5'-ATGCTGCAA TCGTGCTACAA-3'	32838945	N/A
SARS-CoV-2 N R: 5'- GAATGCCGCTTGCTC-3'	32838945	N/A
SARS-CoV-2 N Probe: 5'-/56-FAM/ TCAAGGAAC/ZEN/AACATTGCCAA/ 3IABkFQ/-3'	32838945	N/A
Pierce Biotin	ThermoFisher Scientific	Cat# 29129 -Lot# UH285256
EZ-Link NHS-PEG4-Biotin, No-Weigh Format	ThermoFisher Scientific	Cat# A39259 Lot# VD297193
Calf thymus DNA	ThermoFisher Scientific	Cat# 15633019
Cardiolipin solution from bovine heart	Sigma-Aldrich	Cat# SRE0029
Ultrapure flagellin from <i>S. typhimurium</i>	Invivogen	Cat# tlrl-epstfla-5
Recombinant Human Insulin	Sigma-Aldrich	Cat# I2643
LPS from <i>E. coli</i> O55:B5	Sigma-Aldrich	Cat# L2880
Keyhole Limpet Hemocyanin	Millipore	Cat# 374825
PEI 25K, Transfection Grade	Polysciences	Cat# 23966-2
Super Aquablue ELISA substrate	ThermoFisher Scientific	Cat# 00-4203-58
EasySep Buffer	StemCell Technologies	Cat#20144
Pierce Protein A agarose	ThermoFisher Scientific	Cat# 20334
Anti-SARS-CoV-2 monoclonal antibodies	This paper	Table S7
Critical commercial assays		
Chromium Single Cell A Chip Kit	10X Genomics	Cat# PN-120236
Chromium Single Cell 5' Feature Barcode Library Kit	10X Genomics	Cat# 100080
Chromium Single Cell 5' Library & Gel Bead Kit	10X Genomics	Cat# PN-1000006
Chromium Single Cell 5' Library Construction Kit	10X Genomics	Cat# PN-1000020
Chromium Single Cell V(D)J Enrichment Kit Human B Cell	10X Genomics	Cat# PN-1000016
Chromium i7 Multiplex Kit	10X Genomics	Cat# PN-120262
Chromium i7 Multiplex Kit N, Set A	10X Genomics	Cat# PN-1000084
NextSeq 500/550 High Output Kit v2.5 (150 Cycles)	Illumina	Cat# 20024907
Agilent High Sensitivity DNA Kit	Agilent	Cat# 5067-4626

(Continued on next page)

Continued

REAGENT or RESOURCE	SOURCE	IDENTIFIER
MagMAX-96 Viral RNA Isolation Kit	Thermo Fisher	Cat# AM1836
MagMAX mirVana Total RNA Isolation Kit	Thermo Fisher	Cat# A27828
TaqMan RNA-to-Ct 1-Step Kit	Thermo Fisher	Cat# 4392939
Deposited data		
Antibody sequences	This paper	Gene Expression Omnibus (GEO) GSE171703 and GSM5231088– GSM5231123
Experimental models: cell lines		
HEK293T Cell Line	ATCC	Cat# CRL-11268
Vero E6/TMPRSS2	Japanese Collection of Research Bioresources (JCRB)	https://cellbank.nibiohn.go.jp/~cellbank/ en/search_res_det.cgi?ID=8668
Experimental models: organisms/strains		
Mouse: 2B6.Cg-Tg(K18-ACE2)2Prlnn/J	The Jackson Laboratory	Cat# 034860; RRID:IMSR_JAX:03486
Syrian golden hamsters (HsdHan®:AURA)	Envigo	Item #8902F
Recombinant DNA		
IgG AbVec Plasmid	Patrick Wilson's Laboratory Stock	N/A
Igκ AbVec Plasmid	Patrick Wilson's Laboratory Stock	N/A
Igλ AbVec Plasmid	Patrick Wilson's Laboratory Stock	N/A
Software and algorithms		
MACSQuantifyTyto®Software0.5	MiltenyiBiotecB.V.&Co.KG	N/A
FlowJo 10.7.1	Becton Dickinson & Company	https://www.flowjo.com/solutions/flowjo/ RRID:SCR_008520
Cell Ranger 3.0.2	10x Genomics	https://support.10xgenomics.com/single-cell-gene-expression/software/overview/welcome
Seurat 3.9.9	Stuart et al., 2019	https://satijalab.org/seurat/
IgBlast	N/A	https://www.ncbi.nlm.nih.gov/igblast/ RRID: SCR_002873
ROGUE	Liu et al., 2020	https://github.com/PaulingLiu/ROGUE
IMGT/V-QUEST	Immunogenetics, Marie-Paule Lefranc	http://www.imgt.org/IMGT_vquest RRID: SCR_010749
Jmp (version 15.0)	SAS	https://www.jmp.com/en_us/software.html RRID: SCR_014242
GraphPad Prism (version 9.0.1)	GraphPad Software Inc	http://www.graphpad.com/ RRID: SCR_002798
LinQ-View 0.9.9	Li*, Dugan*, & Stamper* et al., SSRN: https://ssrn.com/abstract=3797273	https://wilsonimmunologylab.github.io/ LinQView/
Circlize 0.4.12	N/A	https://cran.r-project.org/web/packages/ circlize/

RESOURCE AVAILABILITY**Lead contact**

Further information and requests for resources and reagents should be directed to and will be fulfilled by the Lead Contact, Patrick C. Wilson (wilsonp@uchicago.edu).

Materials availability

We are glad to share mAbs with reasonable compensation by the requestor for processing and shipping.

Data and code availability

All single cell B cell 5', VDJ, and antigen probe libraries generated in this study have been deposited to Gene Expression Omnibus: GSE171703 and GSM5231088–GSM5231123. Our dataset and supplementary tables are also available from Mendeley Data: <https://doi.org/10.17632/3jdywv5jrv.3>.

EXPERIMENTAL MODEL AND SUBJECT DETAILS

Human materials

All studies were performed with the approval of the University of Chicago institutional review board IRB20-0523 and University of Chicago, University of Wisconsin-Madison, and Washington University in St. Louis institutional biosafety committees. Informed consent was obtained after the research applications and possible consequences of the studies were disclosed to study subjects. This clinical trial was registered at [ClinicalTrials.gov](#) with identifier NCT04340050, and clinical information for patients included in the study is detailed in [Tables S1–S3](#). Convalescent leukoreduction filter donors were 18 years of age or older, eligible to donate blood as per standard University of Chicago Medicine Blood Donation Center guidelines, had a documented COVID-19 polymerase chain reaction (PCR) positive test, and complete resolution of symptoms at least 28 days prior to donation. Severe acute infected blood donors were 18 years of age or older and blood was collected per standard University of Chicago Medical Center guidelines. Subjects had a documented COVID-19 polymerase chain reaction (PCR) positive test, were hospitalized, and had been scheduled to receive an infusion of convalescent donor plasma. Four blood draws were collected both before and after plasma infusion, at days 0, 1, 3, and 14. PBMCs were collected from leukoreduction filters or blood draws within 2 hours post-collection and, if applicable, flushed from the filters using sterile 1X Phosphate-Buffered Saline (PBS, GIBCO) supplemented with 0.2% Bovine Serum Albumin (BSA, Sigma). Lymphocytes were purified by Lymphoprep Ficoll gradient (Thermo Fisher) and contaminating red blood cells were lysed by ACK buffer (Thermo Fisher). Cells were frozen in Fetal Bovine Serum (FBS, GIBCO) with 10% Dimethyl sulfoxide (DMSO, Sigma) prior to downstream analysis. On the day of sorting, B cells were enriched using the human pan B cell EasySep™ enrichment kit (STEMCELL).

METHOD DETAILS

Recombinant proteins and probe generation

SARS-CoV-2 and Hanta PUUV proteins were obtained from the Krammer laboratory at Mt. Sinai, the Joachimiak laboratory at Argonne, and the Fremont laboratory at Washington University. pCAGGS expression constructs for the spike protein, spike RBD, and hanta PUUV were obtained from the Krammer lab at Mt. Sinai and produced in house in Expi293F suspension cells (Thermo Fisher). Sequences for the spike and RBD proteins as well as details regarding their expression and purification have been previously described ([Amanat et al., 2020](#); [Stadlbauer et al., 2020](#)). Proteins were biotinylated for 2 hours on ice using EZ-Link Sulfo-NHS-Biotin, No-Weigh Format (Thermo Fisher) according to the manufacturer's instructions, unless previously Avi-tagged and biotinylated (ORF8 protein, Fremont laboratory). Truncated cDNAs encoding the Ig-like domains of ORF8 were inserted into the bacterial expression vector pET-21(a) in frame with a biotin ligase recognition sequence at the c-terminus (GLNDIFEAQKIEWHE). Soluble recombinant proteins were produced as described previously ([Nelson et al., 2005](#)). In brief, inclusion body proteins were washed, denatured, reduced, and then renatured by rapid dilution following standard methods ([Nelson et al., 2014](#)). The refolding buffer consisted of 400 mM arginine, 100 mM Tris-HCl, 2 mM EDTA, 200 μM ABESF, 5 mM reduced glutathione, and 500 μM oxidized glutathione at a final pH of 8.3. After 24 hr, the soluble-refolded protein was collected over a 10 kDa ultrafiltration disc (EMD Millipore, PLGC07610) in a stirred cell concentrator and subjected to chromatography on a HiLoad 26/60 Superdex S75 column (GE Healthcare). Site specific biotinylation with BirA enzyme was done following the manufacturer's protocol (Avidity) except that the reaction buffer consisted of 100mM Tris-HCl (pH7.5) 150 mM NaCl, with 5mM MgCl₂ in place of 0.5 M Bicine at pH 8.3. Unreacted biotin was removed by passage through a 7K MWCO desalting column (Zeba spin, Thermo Fisher). Full-length SARS-CoV-2 NP was cloned into pET21a with a hexahistidine tag and expressed using BL21(DE3)-RIL *E. coli* in Terrific Broth (bioWORLD). Following overnight induction at 25°C, cells were lysed in 20 mM Tris-HCl pH 8.5, 1 M NaCl, 5 mM β-mercaptoethanol, and 5 mM imidazole for nickel-affinity purification and size exclusion chromatography. Endemic HCoV spike proteins (HCoV-229E, HCoV-NL63, HCoV-HKU1, and HCoV-OC43) were purchased from Sino Biological. Biotinylated proteins were then conjugated to Biolegend TotalSeq PE streptavidin (PE-SA), APC streptavidin (APC-SA), or non-fluorescent streptavidin (NF-SA) oligos at a 0.72:1 molar ratio of antigen to PE-SA, APC-SA, or NF-SA. The amount of antigen was chosen based on a fixed amount of 0.5 μg PE-SA, APC-SA, or NF-SA and diluted in a final volume of 10 μL. PE-SA, APC-SA, or NF-SA was then added gradually to 10 μL biotinylated proteins 5 times on ice, 1 μL PE-SA, APC-SA, or NF-SA (0.1 mg/ml stock) every 20 minutes for a total of 5 μL (0.5 μg) PE-SA, APC-SA, or NF-SA. The reaction was then quenched with 5 μL 4mM Pierce biotin (Thermo Fisher) for 30 minutes for a total probe volume of 20 μL. Probes were then used immediately for staining.

Antigen-specific B cell sorting

PBMCs were thawed and B cells were enriched using EasySep™ pan B cell magnetic enrichment kit (STEMCELL). B cells were stained with a panel containing CD19 PE-Cy7 (Biolegend), IgM APC (Southern Biotech), CD27 BV605 (Biolegend), CD38 BB515 (BD Biosciences), and CD3 BV510 (BD Biosciences). B cells were stained with surface stain master mix and each COVID-19 antigen probe for 30 minutes on ice in 1X PBS supplemented with 0.2% BSA and 2 mM Pierce Biotin. Cells were stained with probe at a 1:100 dilution (NP, ORF8, RBD, PUUV, empty PE-SA) or 1:200 dilution (spike, endemic HCoV spikes). Cells were subsequently washed with 1X PBS 0.2% BSA and stained with Live/Dead BV510 (Thermo Fisher) in 1X PBS for 15 minutes. Cells were washed again and re-suspended at a maximum of 4 million cells/mL in 1X PBS supplemented with 0.2% BSA and 2 mM Pierce Biotin for downstream cell sorting using the MACSQuantTyto cartridge sorting platform (Miltenyi). Cells that were viable/CD19⁺/antigen-PE⁺ or viable/CD19⁺/antigen-APC⁺ were

sorted as probe positive. The PE⁺ and APC⁺ gates were drawn by use of FMO controls. Cells were then collected from the cartridge sorting chamber and used for downstream 10X Genomics analysis.

10X Genomics library construction

VDJ, 5', and probe feature libraries were prepared using the 10X Chromium System (10X Genomics). The Chromium Single Cell 5' Library and Gel Bead v2 Kit, Human B Cell V(D)J Enrichment Kit, and Feature Barcode Library Kit were used. All steps were followed as listed in the manufacturer's instructions. Specifically, user guide CG000186 Rev D was used. Severe acute infected samples were pooled post-sort and hashtags (Biologend), and run as a single sample, to account for low cell numbers. Final libraries were pooled and sequenced using the NextSeq550 (Illumina) with 26 cycles apportioned for read 1, 8 cycles for the i7 index, and 134 cycles for read 2.

Computational analyses for single cell sequencing data

We adopted Cell Ranger (version 3.0.2) for raw sequencing processing, including 5' gene expression analysis, antigen probe analysis, and immunoprofiling analysis of B cells. Based on Cell Ranger output, we performed downstream analysis using Seurat (version 3.9.9, an R package, for transcriptome, cell surface protein and antigen probe analysis) and IgBlast (version 1.15, for immunoglobulin gene analysis). For transcriptome analysis, Seurat was used for cell quality control, data normalization, data scaling, dimension reduction (both linear and non-linear), clustering, differential expression analysis, batch effects correction, and data visualization. Unwanted cells were removed according to the number of detectable genes (number of genes < 200 or > 2500 were removed) and percentage of mitochondrial genes for each cell. A soft threshold of percentage of mitochondrial genes was set to the 95th percentile of the current dataset distribution, and the soft threshold was subject to a sealing point of 10% as the maximum threshold in the case of particularly poor cell quality. Transcriptome data were normalized by a log-transform function with a scaling factor of 10,000 whereas cell surface protein and antigen probe were normalized by a centered log-ratio (CLR) normalization. We used variable genes in principal component analysis (PCA) and used the top 15 principal components (PCs) in non-linear dimension reduction and clustering. High-quality cells were then clustered by Louvain algorithm implemented in Seurat under the resolution of 0.6. Differentially expressed genes for each cell cluster were identified using a Wilcoxon rank-sum test implemented in Seurat. Batch effects correction analysis was performed using an Anchor method implemented in Seurat to remove batch effects across different datasets. All computational analyses were performed in R (version 3.6.3).

ROGUE scoring

To assess the quality of B cell subsets identified in this study we used ROGUE scoring, an entropy-based metric for assessing the purity of single cell populations, adapted from a previous study (Liu et al., 2020). The expression entropy for each gene was calculated using "SE_fun" from the "ROGUE" package (version 1.0). Based on the expression entropy, the ROGUE score for each cluster was calculated using the "rogue" function from the same package with parameters "platform" set to "UMI" and "span" set to 0.6.

Antigen probe reactivity assignment

Antigen probe signals were normalized by a centered log-ratio transformation individually for each subject. All B cells were subsequently clustered into multiple probe-specific groups according to their normalized probe signals. By investigating all normalized antigen-probe binding signals, we arbitrarily set a threshold equal to 1 for all normalized probe signals to distinguish probe binding cells as "positive" or "negative." Cells that were negative to all probes were clustered into the "negative" group; those positive to only one probe were clustered into corresponding probe-specific groups; and those that were positive to multiple probes were further investigated. Only cells whose top hit probe value was at least two-fold greater than their second hit probe value were clustered into the top hit probe-specific group; others were clustered into the "multi-reactive" group that indicates non-specific cells. To account for the inclusion of endemic HCoV spike protein reactivity in some samples, cells positive to both SARS2 spike and endemic spike were further clustered into a group we assigned as "spike cross-reactive" in the code. For samples in which we included separate SARS2 spike and RBD oligo tags, we placed cells positive to both SARS2 spike and SARS2 RBD into the "spike" group.

Gene module scoring

Scores for B cell-genotype-related gene modules (e.g., MBC score, naive score, ASC score, and GC emigrant score) were calculated using the "AddModuleScore" function from the Seurat package (Stuart et al., 2019). The naive score was calculated based on the genes *BACH2*, *ZBTB16*, *APBB2*, *SPRY1*, *TCL1A*, and *IKZF2*; the MBC score was calculated based on the genes *CD27*, *CD86*, *RASSF6*, *TOX*, *TRERF1*, *TRPV3*, *POU2AF1*, *RORA*, *TNFRSF13B*, *CD80*, and *FCRL5*; the ASC score was calculated based on genes *PRDM1*, *MANF*, *XBP1*, *IL6R*, *BCL6*, *IRF4*, *TNFRSF17*, and *CD38*; and the GC emigrant score was calculated based on genes *NT5E*, *MKI67*, *CD40*, *CD83*, *TNFRSF13B*, *MAP3K8*, *MAP3K1*, and *FAS*.

Selection of antibodies for mAb synthesis

Representative antibodies from each subject were chosen for synthesis by choosing random samplings of B cells that bound to a given antigen probe with higher intensity relative to all other probes. B cells with varying ranges of probe-binding intensities were chosen for confirmation by ELISAs. In addition, B cells representing select public clonal expansions were also chosen for cloning.

B cells binding to all probes in a polyreactive manner were also chosen and validated for polyreactivity by polyreactivity ELISA (see methods below).

Monoclonal antibody generation

Immunoglobulin heavy and light chain genes were obtained by 10X Genomics VDJ sequencing analysis and monoclonal antibodies (mAbs) were synthesized by Integrated DNA Technologies. Cloning, transfection, and mAb purification have been previously described ([Guthmiller et al., 2019](#)). Briefly, sequences were cloned into human IgG1 expression vectors using Gibson assembly, and heavy and light genes were co-transfected into 293T cells (Thermo Fisher). Secreted mAbs were then purified from the supernatant using protein A agarose beads (Thermo Fisher).

Enzyme-linked immunosorbent assay (ELISA)

High-protein binding microtiter plates (Costar) were coated with recombinant SARS-CoV-2 proteins at 2 µg/ml in 1X PBS overnight at 4°C. Plates were washed the next morning with 1X PBS 0.05% Tween and blocked with 1X PBS containing 20% fetal bovine serum (FBS) for 1 hour at 37°C. Antibodies were then serially diluted 1:3 starting at 10 µg/ml and incubated for 1 hour at 37°C. Horseradish peroxidase (HRP)-conjugated goat anti-human IgG antibody diluted 1:1000 (Jackson Immuno Research) was used to detect binding of mAbs, and plates were subsequently developed with Super Aquablue ELISA substrate (eBiosciences). Absorbance was measured at 405 nm on a microplate spectrophotometer (BioRad). To standardize the assays, control antibodies with known binding characteristics were included on each plate and the plates were developed when the absorbance of the control reached 3.0 OD₄₀₅ units. All experiments were performed in duplicate 2–3 times.

Polyreactivity ELISA

Polyreactivity ELISAs were performed as previously described ([Andrews et al., 2015](#); [Bunker et al., 2017](#); [Guthmiller et al., 2020](#)). High-protein binding microtiter plates (Costar) were coated with 10 µg/ml calf thymus dsDNA (Thermo Fisher), 2 µg/ml *Salmonella enterica* serovar Typhimurium flagellin (Invitrogen), 5 µg/ml human insulin (Sigma-Aldrich), 10 µg/ml KLH (Invitrogen), and 10 µg/ml *Escherichia coli* LPS (Sigma-Aldrich) in 1X PBS. Plates were coated with 10 µg/ml cardiolipin in 100% ethanol and allowed to dry overnight. Plates were washed with water and blocked with 1X PBS/0.05%Tween/1mM EDTA. MAbs were diluted 1 µg/ml in PBS and serially diluted 4-fold, and added to plates for 1.5 hours. Goat anti-human IgG-HRP (Jackson Immunoresearch) was diluted 1:2000 in PBS/0.05%Tween/1mM EDTA and added to plates for 1 hour. Plates were developed with Super Aquablue ELISA substrate (eBioscience) until the positive control mAb, 3H9 ([Shlomchik et al., 1987](#)), reached an OD₄₀₅ of 3. All experiments were performed in duplicate.

Neutralization assay

The SARS-CoV-2/UW-001/Human/2020/Wisconsin (UW-001) virus was isolated from a mild case in February 2020 and used to assess neutralization ability of monoclonal antibodies (mAbs). Virus (~500 plaque-forming units) was incubated with each mAb at a final concentration of 10 µg/ml. After a 30-minute incubation at 37°C, the virus/antibody mixture was used to inoculate Vero E6/TMPRSS2 cells seeded a day prior at 200,000 cells per well of a TC12 plate. After 30 minutes at 37°C, cells were washed three times to remove any unbound virus, and media containing antibody (10 µg/ml) was added back to each well. Two days after inoculation, cell culture supernatant was harvested and stored at –80°C until needed. A non-relevant Ebola virus GP mAb and PBS were used as controls.

To determine the amount of virus in the cell culture supernatant of each well, a standard plaque-forming assay was performed. Confluent Vero E6/TMPRSS2 cells in a TC12 plate were infected with supernatant (undiluted, 10-fold dilutions from 10⁻¹ to 10⁻⁵) for 30 minutes at 37°C. After the incubation, cells were washed three times to remove unbound virus and 1.0% methylcellulose media was added over the cells. After an incubation of three days at 37°C, the cells were fixed and stained with crystal violet solution in order to count the number plaques at each dilution and determine virus concentration given as plaque-forming units (PFU)/ml.

In vivo protection assays

To evaluate the efficacy of RBD and NP monoclonal antibodies (mAbs) *in vivo*, groups of 4–5-week-old female Syrian golden hamsters (four animals in each group) were infected with SARS-CoV-2 at a dose of 10³ PFU by intranasal inoculation. One day later, the hamsters were treated by intraperitoneal injection with one of the mAbs at 5 mg/kg. Control groups of hamsters were injected with either sterile PBS or a non-relevant mAb (Ebola glycoprotein 133/3.16). Weights were recorded daily. Four days after the infection, nasal turbinate and lung samples were collected to determine viral loads in these tissues by standard plaque assay on Vero E6/TMPRSS2 cells. All animal studies were conducted under BSL-3 containment with an approved protocol reviewed by the Institutional Animal Care and Use Committee at the University of Wisconsin.

Studies with mice were carried out in accordance with the recommendations in the Guide for the Care and Use of Laboratory Animals of the National Institutes of Health. The protocols were approved by the Institutional Animal Care and Use Committee at the Washington University School of Medicine (assurance number A3381–01). Virus inoculations were performed under anesthesia that was induced and maintained with ketamine hydrochloride and xylazine, and all efforts were made to minimize animal suffering. To evaluate the efficacy of ORF8 mAbs *in vivo*, eight-week-old heterozygous female K18-hACE c57BL/6J mice (strain: 2B6.Cg-Tg(K18-ACE2)2Prlmn/J) received 200 µg of each indicated mAb by intraperitoneal injection one day prior to intranasal inoculation

with 10^3 PFU of SARS-CoV-2 (n-CoV/USA_WA1/2020 strain). Weight change was monitored daily and lungs were harvested at 7 days post-infection. Viral RNA levels in lung homogenates were determined by qRT-PCR quantifying N gene copy number and compared to a standard curve as described previously ([Winkler et al., 2020](#)).

QUANTIFICATION AND STATISTICAL ANALYSIS

All statistical analysis was performed using Prism software (Graphpad Version 9.0) or R. Chi-square tests were corrected for multiple comparisons using post hoc Chi-square test. Sample sizes (n) are indicated in corresponding figures or figure legends. The number of biological repeats for experiments and specific tests for statistical significance used are indicated in the figure legends. P values less than or equal to 0.05 were considered significant. * $p < 0.05$, ** $p < 0.01$, *** $p < 0.001$, **** $p < 0.0001$.